

# Hidden massive eclipsing binaries in red supergiant systems

## The hierarchical triple system KQ Puppis and other candidates\*

D. Jadlovský<sup>1,2</sup>, L. Molnár<sup>3,4,5</sup>, A. Ercolino<sup>6</sup>, M. Bernini-Peron<sup>7</sup>, A. Mérand<sup>2</sup>, J. Krtička<sup>1</sup>, L. Wang<sup>9</sup>, R.Z. Ádám<sup>3,4</sup>, D. Baade<sup>2</sup>, G. González-Torà<sup>7</sup>, T. Granzer<sup>10</sup>, J. Janák<sup>1</sup>, J. Kolář<sup>1</sup>, K. Kravchenko<sup>11</sup>, N. Langer<sup>5</sup>, L. M. Oskinova<sup>12</sup>, D. Pauli<sup>13</sup>, V. Ramachandran<sup>7</sup>, A. C. Rubio<sup>14</sup>, A.A.C. Sander<sup>7,8</sup>, K.G. Strassmeier<sup>10</sup>, M. Weber<sup>10</sup>, M. Wittkowski<sup>2</sup>, R. Brahm<sup>15,16</sup>, V. Schaffenroth<sup>17</sup>, L. Vanzi<sup>18</sup>, and M. Skarka<sup>19</sup>

(Affiliations can be found after the references)

### ABSTRACT

**Context.** The majority of massive stars are part of binary systems that may interact during their evolution. This has important consequences for systems in which one star develops into a Red supergiant (RSG); however, not many RSGs are known binaries, and only a few have constrained orbital parameters.

**Aims.** We aim to better characterize and constrain the properties of some of the known RSGs in binaries, inspired by recent observations where these RSGs transitioned to an earlier spectral type, likely following a major interaction event with their companions.

**Methods.** We first focus on the VV Cephei type RSG KQ Pup (made up of a RSG, KQ Pup A, and a B-type companion, KQ Pup B, with an orbital period of 26 yr), where we have enough data to constrain the system's properties. We use archival photometry and UV spectroscopy, along with newly taken optical spectra and interferometric data with VLTI-GRAVITY. For KQ Pup, as well as for all other Galactic RSGs, we also analyzed the available TESS photometry.

**Results.** Using TESS light curves, we discovered eclipses with a period of 17.2596 d, associated with KQ Pup B, making it a binary. We will refer to the two components as KQ Pup Ba and KQ Pup Bb. Meanwhile, the detection of the hydrogen Bry line with VLTI-GRAVITY enabled us to track the orbital motion of the KQ Pup Ba+Bb pair and thus to determine the astrometric orbit. The dynamical masses agree with independent estimates from asteroseismology and evolutionary models. The results give a mass of  $\sim 9 M_{\odot}$  for the RSG KQ Pup A and  $\sim 14 M_{\odot}$  for the sum of the hot components Ba+Bb. The observed properties of the system are compatible with coeval hierarchical triple-star, where we constrain the minimum mass of KQ Pup Bb as  $\gtrsim 1.2 M_{\odot}$ .

**Conclusions.** The variability of Balmer lines and the detection of Bry represent a strong signature of Wind Roche Lobe Overflow, with enhanced signatures of disk-accretion to the Ba+Bb pair during the periastron. Meanwhile, TESS light curves show that about  $\sim 10\%$  of known Galactic binary RSGs may be eclipsing hierarchical triple systems, which suggests that a large fraction of other binary RSGs could also be triples.

**Key words.** stars: supergiants – stars: massive – stars: mass-loss – binaries: eclipsing – techniques: interferometric

### 1. Introduction

Red supergiants (RSGs) are a critical point of evolution for massive stars ( $M > 8 M_{\odot}$ ). During the RSG phase, stars experience increased mass loss rates (van Loon et al. 2005), significantly contributing to the dust production in galaxies (Levesque 2017). They may explode as Type IIP/L supernovae (SN), or further evolve and explode as a different type of SN (Smartt et al. 2009). While the effect of the mass loss can significantly alter their final evolution, there are many uncertainties in the mass-loss process. Recently, it has been shown that episodic mass-loss events may be the missing link to explain the mass-loss process, as shown for example through the dimming event of Betelgeuse (e.g., Montargès et al. 2021; Dupree et al. 2022; Humphreys & Jones 2022) and RW Cep (Anugu et al. 2023). The binary interaction can be one of the deciding factors (Ercolino et al. 2024), as the majority of massive stars have a companion that they will interact with at some point during their evolution (Sana et al. 2012). Nonetheless, there are only a few binary RSG systems that are well-characterized (Patrick & Negueruela 2024).

Most of the few well-studied binary RSG systems belong to the VV Cephei type binaries (Cowley 1969), i.e., wide interacting systems with periods from years to decades, which consist of a cool K/M supergiant and early B-type star. The optical spectra show broad emission wings of the Balmer series and many singly-ionized emission lines, including the forbidden emission lines. In the initial sample by Cowley (1969), there were 13 RSGs. Some of the VV Cephei stars also belong to the rare type of  $\zeta$  Aurigae type binaries, i.e., an eclipsing binary system undergoing the chromospheric eclipses phenomenon (Ake & Griffin 2015). In VV Cephei and  $\zeta$  Aurigae binaries, their companions essentially probe the subsonic part of the cool wind, which is otherwise difficult to constrain by observations. This was exploited by Dupree (1986); Dupree & Reimers (1987) for several such systems to study the mass-loss process of red giants and supergiants, based on observations of the wind of the cool star against the spectrum of the hot star (Dupree 1986; Dupree & Reimers 1987). These data were used by Reimers (1975) for determining the widely used mass-loss relation.

Nowadays, the number of identified Galactic RSG binaries has increased considerably. For the most up-to-date list of Galactic RSGs, we consider the list of Galactic RSGs and RSG candidates from Healy et al. (2024), which includes about 79 binaries,

\* Based on observations made with the Very Large Telescope Interferometer (VLTI) at the Paranal Observatory under program 114.27NF.001, (PI: Jadlovský)

out of which 44 are identified as RSGs in SIMBAD<sup>1</sup>. The situation is further improved by newly detected populations of binary RSG+B binaries in the Local Group (Neugent et al. 2018, 2019; Dorda & Patrick 2021; Patrick et al. 2022, 2025), increasing the sample by several dozen binaries. These results allowed us to determine the fraction of RSG binaries to single RSGs,  $\sim 10 - 30\%$  in Magellanic Clouds (Neugent et al. 2020; Dai et al. 2025) and  $\sim 15 - 40\%$  in M31 and M33 (Neugent 2021).

It is not clear what fraction of binary RSGs in these new samples show properties similar to those of the classical VV Cephei binaries. Patrick et al. (2025) spectroscopically studied 16 RSG+B systems in the Small Magellanic Cloud and found that 4 of them also show signatures of being embedded in the wind of the RSG. They also found that in several of their systems, the ages for the RSG star and hot companion disagree, suggesting a past mass transfer, while the rest of the sample can be explained by co-eval evolution. The recent dramatic transition of RSG WOH G64 in the Large Magellanic Cloud to an earlier spectral type (Ohnaka et al. 2024), very likely due to an interaction with its B-type companion (Munoz-Sánchez et al. 2024), demonstrated that binary interaction can indeed have a strong impact on the final evolution. Furthermore, other single RSGs, such as Betelgeuse, were recently hypothesized to have a low-mass companion (Goldberg et al. 2024; MacLeod et al. 2025). Following several non-detections (Goldberg et al. 2025; O’Grady et al. 2025), it seems that the companion has been finally detected via speckle imaging (Howell et al. 2025).

In this work, we report on the discovery of several possible hierarchical triple red supergiant systems identified with the Transiting Exoplanet Survey Satellite (TESS, Ricker et al. 2015). We focus on the VV Cephei-type system KQ Pup, where we have sufficient data to study the system. Based on the discovery of the third component in the KQ Pup system, we adjust the system configuration to A + (Ba+Bb), with A being the RSG. For the other stars in the sample, we list the candidates that will require further observations to confirm or rule out the new companions.

KQ Pup system consists of a RSG component, KQ Pup A (M2Iab, HD 60414), and a B-type star, KQ Pup B (B0V, HD 60415), as classified by Rossi et al. (1992). It is one of the most prominent members of the VV Cephei type binaries and used to be one of the systems with the longest orbital periods known (26 yr, González-Riestra et al. 2002). It is also considered a southern analogue of the more famous VV Cephei star (e.g., Bauer & Bennett 2000), although, unlike VV Cephei, it is not known to undergo atmospheric eclipses. UV and optical spectroscopic properties of the system were described by Altamore et al. (1982, 1992); Rossi et al. (1992); Muratorio et al. (1992), while more recent results from HST and FUSE were also described in González-Riestra et al. (2002, 2003). Cowley (1965) analyzed RV measurements of KQ Pup from 1918-1964 and derived an eccentric orbit, with a period of  $P = 9752 \pm 85$  d, eccentricity  $e = 0.46 \pm 0.03$  and argument of periastron  $w = 202.6 \pm 2.1^\circ$  (conjunctions close to periastron). In a related study, Rossi et al. (1992) expanded on these results and estimated mass ratio  $q = \frac{M_B}{M_A} = 0.8 - 1.2$  and with a semi-major axis  $a \sin(i) = 13.6$  au. For the hot companion, KQ Pup B, they found a spectral type of B0 with  $T_{\text{eff}} = 30\,000$  K. In the most recent study on the KQ Pup system, González-Riestra et al. (2002) derived a revised period of  $P = 9500 \pm 50$  d ( $\sim 26$  yr). In these studies, a distance of  $1400 \pm 200$  pc was assumed (parallax  $\pi \sim 0.71$  mas). However, revised Hipparcos give a parallax  $\pi = 2.12$  mas van

Leeuwen (2007), while Gaia gives  $\pi = 1.36$  mas (Gaia Collaboration et al. 2021). In this work, we adopt a geometric Gaia distance of  $\sim 779$  (693 – 920) pc from Bailer-Jones et al. (2021, hereafter BJ21).

The paper is structured as follows: in Sect. 2 we list interferometric, spectroscopic, and photometric data used in this work, in Sect. 3 we derive more precise parameters of the KQ Pup system, treating it as A+B system, while in Sect. 4 we deduce the likely properties of the third component, KQ Pup Bb, and in Sect. 5 we list the other candidates. Lastly, in Sect. 6, we discuss the classification of RSG binaries and the implications of the newly discovered systems to the evolution of massive stars, while in Sect. 7 we summarize our results.

## 2. Observations and data reduction

### 2.1. Interferometry

We obtained 3 spectro-interferometric observations of KQ Pup using the VLTI-GRAVITY instrument (GRAVITY Collaboration et al. 2017) at Paranal Observatory. The observations are part of the observing programme 114.27NF.001 (PI: Jadlovský) focused on the analysis of the mass-loss process for a large sample of southern RSGs. We used a small configuration of Auxiliary Telescopes (ATs), with baselines between  $\sim 10 - 35$  m. The instrument operates in near-infrared  $K$ -band ( $1.98 - 2.40 \mu\text{m}$ ) and we used the high spectral resolution mode ( $R \sim 4000$ ). For each observation, we observed 2 calibrators using the CAL-SCI-CAL sequence, improving the quality of the calibration. The observing logs and properties of calibrators are listed in Appendix A. Considering the high brightness of KQ Pup ( $K \sim 0.11$  mag), we used the split polarization instrumental mode.

We reduced the raw data of KQ Pup and its calibrators using the *ESO Reflex* workflow for VLTI-GRAVITY in its version 1.9.0<sup>2</sup>. Interferometric visibility of calibrators was used to calibrate the visibility of KQ Pup. The final interferometric calibrated dataset includes the visibilities ( $|V|$ ) and differential phases (DPHI) for six baselines, as well as closure phases (T3PHI) for four telescope triangles.

To analyze the final data, we used Python code Parametric Modeling of Optical Interferometric Data<sup>3</sup> (PMOIRED, Mérand 2022). PMOIRED allows to fit interferometric data with multi-component geometric models, using the least-squares minimization to obtain the best fit. In our case, we use functions for detecting binary signatures in spectral lines, allowing us to perform relative astrometry in the KQ Pup system.

### 2.2. Spectroscopy

To obtain new high-cadence spectral time series of KQ Pup, we used the Stellar Activity (STELLA) echelle spectrograph (SES) mounted on a fully robotic 1.2 m telescope at the Izaña Observatory in Tenerife, which is operated by AIP (Strassmeier et al. 2004, 2010). The resolving power is  $R \approx 55\,000$  with a three-pixel sampling per resolution element. The spectra cover the 390–880 nm wavelength range. Our time series consists of 50 spectra taken between April 2024 and February 2025. Spectra were reduced using the IRAF-based SESDR 4.0 pipeline (Weber et al. 2008, 2012). The determination of radial velocity (RV) is described in Sect. 3.4.

<sup>2</sup> <https://www.eso.org/sci/software/pipelines/gravity/gravity-pipe-recipes.html>

<sup>3</sup> <https://github.com/amerand/PMOIRED>

<sup>1</sup> <https://simbad.cds.unistra.fr/simbad/>

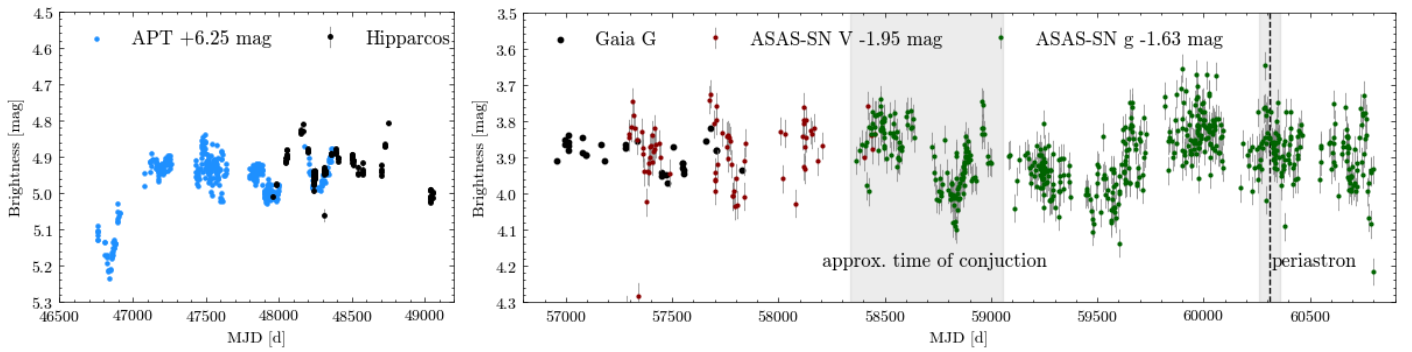


**Fig. 1.** Photometric light curve of KQ Pup, comprising of several archival sources - APT, Hipparcos, Gaia, and ASAS-SN. Other data are shifted to match Hipparcos and Gaia. We also mark an approximate time of conjunction before periastron and periastron in January 2024.

We also took new optical spectra for KQ Pup, as well as other targets (see Table 2) using PLATOSpec<sup>4</sup> (Kabath et al., in prep.) mounted on the ESO 1.52m telescope at the La Silla Observatory, which covers the wavelength range from 380 nm to 680 nm and has a resolving power  $\sim 70\,000$ . By default, data from PLATOSpec are processed using the CERES+ pipeline (Brahm et al. 2017), but for the stars we measured, where emission lines are observed, standard IRAF routines were used. Additionally, we compared to the archival ESPADONS (Manset & Donati 2003) spectra downloaded from the Polarbase database<sup>5</sup> and archival FEROS spectra downloaded via SPLAT<sup>6</sup>.

Lastly, we employed the archival spectra of KQ Pup taken with the International Ultraviolet Explorer (IUE) satellite during 1978–1995. We downloaded IUE spectra from the MAST archive<sup>7</sup>. The total dataset of high-resolution UV spectra for KQ Pup consists of 23 spectra in the short wavelength region (SWP, 1150 – 1980 Å) and 17 in the long wavelength region (LWP, 1850 – 3350 Å). However, some spectra associated with KQ Pup are at a distance of  $\sim 7^\circ$  and  $\sim 48^\circ$ , which we excluded from our analysis, as well as a few low signal-to-noise spectra. See Sect. 3.4 for the determined RVs.

### 2.3. Photometry

We used photometry from TESS (Ricker et al. 2015). We extracted TESS light curves from Full Frame Images (TESS-SPOC, Caldwell et al. 2020) for KQ Pup, as well as other RSG targets (see Sect. 5), using the *lightkurve* package (Lightkurve Collaboration et al. 2018). We inspected observations in every sector and the available reduction pipeline. The chosen primary target, KQ Pup, has been observed in four sectors so far, in Sectors 7, 34, 61, and 88. In all cases, 120 s short-cadence postage-stamp data were collected, so we used these observations for our analysis. Raw light curves and light curves of further eclipse detections for other RSGs, are summarized in Appendix C.

Additionally, for KQ Pup, we use time-domain photometry from the Hipparcos and Gaia space missions (van Leeuwen et al. 1997; Gaia Collaboration et al. 2023) and from the All-Sky Automated Survey for Supernovae (ASAS-SN), using their new saturated stars pipeline (Kochanek et al. 2017; Winecki & Kochanek 2024). Hipparcos and Gaia used their own specific, wide passbands. ASAS-SN data were initially collected in the

Johnson V, and later in the Sloan *g* passband. We also used differential photometry for KQ Pup taken with T2 0.25 m Automatic Photoelectric Telescope (APT) at Fairborn Observatory (Gregory Henry, private communication) at filter V. These observations are summarized in Fig. 1.

## 3. KQ Puppis system

### 3.1. Photometric variability

In Fig. 1, we show the photometric variability of KQ Pup during the last 40 years. The photometric variations are primarily caused by the variability of the RSG, no clear photometric variations related to the 26-yr orbit were identified in the previous studies.

The beginning of the APT light curve in 1986–1987 shows a 0.3 mag dimming event that clearly exceeds the amplitude of oscillations. This event is at least 5 years away from any conjunction or potential eclipse so geometric effects from the companion(s) can be ruled out. The dimming resembles the great dimming event of Betelgeuse (e.g., Montargès et al. 2021), which was caused by partial obscuration by a dense dust cloud.

A frequency analysis of the light curves revealed various low-amplitude periodicities ranging between 85–180 d (0.06–0.14  $\mu$ Hz in frequencies), and possibly extending to even longer periods. However, aliasing from the annual gaps present in the data makes the existence of longer periods questionable, which hinders the accurate determination of the mode content. The variations of the star appear to be more similar to solar-like oscillations seen in luminous RGB stars and M giants, composed of multiple short-lifetime modes, rather than to coherent pulsations (Bányai et al. 2013; Yu et al. 2020; Xiong et al. 2025). Incoherent oscillations in RSG stars have been detected before (Kiss et al. 2006; Joyce et al. 2020). However, mode identification for asteroseismic analysis can be difficult, with the aliasing present in the data.

We therefore decided to treat the star as an oscillating giant and attempted to measure global seismic parameters of the star. The power of asteroseismology lies in the fact that we can extrapolate our helioseismic knowledge and scale the solar values of various physical parameters, including L, M, R,  $T_{\text{eff}}$ , as well as global asteroseismic parameters, to other stars (Kjeldsen & Bedding 1995; Huber et al. 2011). To have a rough estimate on the possible seismic mass range of KQ Pup A, we first determined the frequency of maximum oscillation amplitude, or  $\nu_{\text{max}}$  parameter. As a first estimate, we can use simply the midpoint of the clearly identified periodicities in frequency space, which

<sup>4</sup> <https://stel.asu.cas.cz/plato/spectrograph.html>

<sup>5</sup> <https://www.polarbase.ovgso.fr/>

<sup>6</sup> <https://www.g-vo.org/pmwiki/About/SPLAT>

<sup>7</sup> <https://mast.stsci.edu/portal/Mashup/Clients/Mast/Portal.html>

yields an approximate value of  $\nu_{\max} = 0.12 \pm 0.02 \mu\text{Hz}$  (or  $97^{+20}_{-14}$  d in period). Unfortunately, at this point, we could not determine  $\Delta\nu$ , the frequency spacing between successive radial overtones, clearly.

Multiple scaling relations have been defined in the literature, but since we only have an estimate for  $\nu_{\max}$ , we chose the following scaling relation:

$$\frac{M}{M_{\odot}} = \left( \frac{f_{\nu} \nu_{\max}}{\nu_{\max, \odot}} \right) \left( \frac{L}{L_{\odot}} \right) \left( \frac{T_{\text{eff}}}{T_{\text{eff}, \odot}} \right)^{-7/2}, \quad (1)$$

where the solar values are  $\nu_{\max, \odot} = 3090 \pm 30 \mu\text{Hz}$  and  $T_{\text{eff}, \odot} = 5772 \text{ K}$ , following Huber et al. (2011). The  $f_{\nu}$  parameter is a correction factor accounting for the structural differences between the target and the Sun. Here we set it to  $f_{\nu} = 1.05$ , based on the results of Ash et al. (2025), who found that this type of scaling relation underestimates the masses at the lowest  $\nu_{\max}$  values. However, this analysis was based on low-mass RGB stars: the correction factors for RSG stars have not been tested yet. We use  $T_{\text{eff}} = 3660 \pm 170 \text{ K}$  (Healy et al. 2024) and two different values for the luminosity:  $\log L/L_{\odot} = 4.55$  and  $\log L = 4.77$  based on Healy et al. (2024) and Rossi et al. (1992), respectively.

This preliminary estimate gives us two seismic mass ranges for KQ Pup A:  $M_{\text{low}L} = 7.1 \pm 1.7 M_{\odot}$  and  $M_{\text{hi}L} = 11.8 \pm 2.8 M_{\odot}$  for the low and high luminosity values. These large uncertainties can be lowered with a more accurate determination of  $\nu_{\max}$  and with stronger constraints on the luminosity of the RSG. A detailed asteroseismic analysis of KQ Pup A will be the topic of a separate paper.

### 3.2. Spectral variability

A multi-wavelength spectral analysis is possible due to an abundance of archival IUE spectra covering most of the 26-year orbital period (1978–1995). Following the most recent periastron in January 2024, we have also obtained new high-resolution spectra in the optical region with STELLA and PLATOSpec, as well as in the near-IR with VLTI-GRAVITY. As shown by Rossi et al. (1998), but also recently by Neugent et al. (2018), for RSG+B binaries, the spectral energy distribution at wavelengths longer than  $\sim 4000 \text{ \AA}$  is typically dominated by the RSG. Nonetheless, for systems where the companion is embedded in the dense, cool shocked wind of the RSG, as in the case of VV Cep or systems studied by Patrick et al. (2025), the hot companion may not be directly observed in the spectrum even at below  $\sim 4000 \text{ \AA}$ .

At longer wavelengths, for VV Cephei stars, the contribution from the hot component can still be seen as double-peaked emission profiles in the Balmer series, which is shown in Fig. B.1. The V/R ratios (ratio between violet and red shifted emission peak) of Balmer lines depend on the 26-year orbital phase. The emission components become the weakest around the apastron ( $\phi \sim 0.5$ ), and nearly fully disappear except for H $\alpha$ . Meanwhile, the emission components become the strongest near periastron, showing strong violet-shifted emission for all transitions until the Balmer break, appearing as reverse P Cygni. At periastron (phase  $\phi \sim 0$ ), V/R ratio quickly goes from  $> 1$  to  $< 1$ . The highest Balmer transitions are typically not detected in RSG spectra. We compare the profiles to new RSG+B binaries by Neugent et al. (2019). Unlike in their case, here, the Balmer lines are narrow and do not show wide rotationally broadened absorption profiles typical of hot stars. That suggests that the hot companion, KQ Pup B, is likely also embedded in the dense circumstellar environment (CSM) and cannot be directly seen in the optical spectra, while the narrow absorptions likely form in the

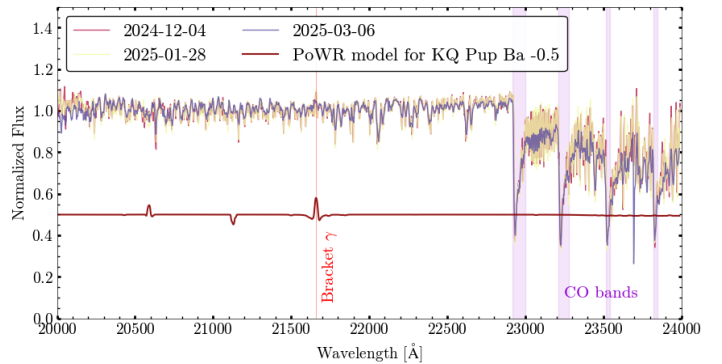


**Fig. 2.** Near-IR spectra from VLTI GRAVITY. There are prominent spectral features related to RSGs, such as the CO bands at  $\sim 2.29 - 2.4 \mu\text{m}$ . Based on the interferometric properties, the only feature clearly corresponding to the hot companion (KQ Pup Ba) is the hydrogen Bry feature at  $2.167 \mu\text{m}$ . The only other two prominent lines of the hot companion in the region, He I at  $2.059 \mu\text{m}$  and  $2.113 \mu\text{m}$ , are not detected.

wind near the hot companion. Optical spectra also include forbidden emission lines (primarily [Fe II]). Other prominent lines of hot stars, He I lines, are very weak in the optical spectrum and only show typical RSG profiles. But below  $\sim 4000 \text{ \AA}$ , the profiles may be associated with the hot component, most notably the rotationally broadened He I 3819  $\text{\AA}$  line, as also noted by Rossi et al. (1992). We also note that Na I doublet shows a strong secondary component in all observations, again related to the orbital period, with the sharp central component not moving and the wider typical RSG component moving along the phase  $\phi$ , see Fig. B.6.

At shorter wavelengths, the hot companion dominates, and thus UV spectra can be used to study more of its properties, especially related to its wind. As analyzed in detail in the aforementioned studies, there are several line systems present, superimposed on each other. First, in the far UV, there are broad absorptions of ionized resonance lines (e.g., C II, N V), as well as other lines typical of the wind of hot stars. There are also absorptions of excited lines of doubly-ionized metals (e.g., Fe III). Second, in the near UV, there are many P Cygni profiles of singly-ionized elements present (primarily Fe II), where the absorption part likely corresponds to the RSG wind as seen against the hot companion, and the emission part is likely produced in the cool wind of the RSG ionized by the radiation of the hot companion. In UV, the appearance of the spectrum is strongly variable with the orbital phase  $\phi$ , as shown in Fig. B.2. Emission lines of permitted transitions, including those in P Cygni profiles, move to shorter wavelengths during the orbital phase  $\phi$ , while the absorption cores of Fe II P Cygni profiles move to longer wavelengths (resulting in reverse P Cygni appearance near the periastron). Some broad lines corresponding to doubly ionized elements in far UV (e.g., Fe III near  $\sim 1900 \text{ \AA}$ ) nearly disappear near the apastron. Meanwhile, prominent double-peaked UV emission lines (such as Mg II and Fe II multiplets at  $\sim 2800 \text{ \AA}$  and  $\sim 1787 \text{ \AA}$ , respectively) also show a clear relation to the orbital phase.

Additionally, in Fig. 2, we show the near-infrared  $K$ -band spectrum obtained with VLTI-GRAVITY. Similar to the optical region, the entire spectrum is dominated by the RSG, showing typical RSG features, such as strong CO molecular bands and neutral metals. The only line clearly associated with the hot companion is the hydrogen Brackett gamma (Bry) line at  $2.167 \mu\text{m}$ .

### 3.3. Model atmospheres fitting

To estimate the stellar parameters of the B-star, we compared the observed IUE spectra to synthetic spectra from atmosphere models computed with the Potsdam Wolf-Rayet (PoWR) model atmosphere code (Gräfener et al. 2002; Sander et al. 2015). PoWR solves the radiative transfer (RT) simultaneously with the rate equations (i.e., in non-LTE) in the comoving frame of a spherically symmetric, stationary expanding atmosphere (i.e., an outflowing wind).

As a starting point, we selected a B-star model from the Galactic OB-Vd3 grid (Hainich et al. 2019, Pauli et al. subm.), namely  $T_* = 20.0$  kK and  $\log g = 3.6$ . The choice of  $T_*$  was motivated by the UV spectral signatures – see below. To improve the UV fit, we then calculate a tailored model, which is compared to the median IUE SWP spectra. As the optical spectrum of KQ Pup is dominated by the RSG (KQ Pup A), we do not have clear diagnostics for the surface gravity ( $\log g$ ) for KQ Pup B, which prevents the determination of the stellar mass. The chosen grid model has  $\log g$  typical of B dwarfs of similar temperatures (e.g., Daflon et al. 2003; Ramachandran et al. 2019). By fitting the UV pseudo-continuum and He I lines below 4000 Å (e.g., He I 3819Å), we find a projected rotation velocity  $v \sin i = 190 \pm 70$  km s $^{-1}$ . To obtain the luminosity  $L$  of KQ Pup B, we fit the synthetic model SED of the B-star to the flux-calibrated IUE spectra, considering a distance of 780 pc from Gaia (BJ21) – see Fig. B.3. We estimate  $\log L/L_\odot \sim 3.95$  and a reddening of  $E(B-V) = 0.30$  with  $R_V = 3.3$  assuming the extinction curve from Fitzpatrick (1999). The reddening was obtained based on the 2175 Å absorption bump.

We notice the presence of C II 1335, Si IV 1400, C IV 1550, and Al III 1855. The simultaneous presence of these lines hints at a temperature of  $\sim 20$  kK. However, these diagnostic lines do not show up as typical P Cygni profiles, which are observational signatures of spherically symmetric outflows – see Fig. B.4. Instead, the profiles are broad absorptions (extending up to  $\sim 200$  km s $^{-1}$ ), seemingly centered around the respective transition wavelengths and asymmetrically redshifted, which may suggest a different wind geometry. In the optical, we also notice a similar behavior in the Balmer lines with inverted P Cygni profiles (see FEROS spectra from 1997 in Fig. B.1). Such behavior can be explained by the geometry of the system: i.e., the wind of the B star interacts with the dense RSG wind before it develops to its terminal velocity. Winds in such systems of RSG + hot companion were discussed in, e.g., Dupree & Reimers (1987). The lack of clear P Cygni profiles throughout the UV also limits a precise determination of mass-loss rates ( $\dot{M}$ ). The grid models by default assume  $\dot{M}$  follows the Vink et al. (2001) mass-loss recipe divided by 3, which yields  $\log \dot{M} = -8.5$  in this case. For reproducibility, we list all the input stellar and wind parameters in Table 1.

In Fig B.4, we also notice the presence of a strong N V 1240 doublet, which is incompatible with the derived atmosphere temperature, as this line would require a higher temperature. In fact, this profile can only appear in early B and O stars in the presence of X-rays or extreme UV radiation as an extra source of ionization (e.g., Oskinova 2016; Puebla et al. 2016). As a presumably mid-type B-star, a typical amount of X-ray luminosity cannot produce such a strong profile (see Bernini-Peron et al. 2023, 2024). In our modeling, the inclusion of X-rays (based on  $\log L_X/L \sim -6.5$  from Merloni et al. 2024) helped as an extra source of ionization to strengthen C IV 1550, which cannot be produced without X-rays in such a temperature.

### 3.4. Radial velocity

In this work, we focus on identifying line systems corresponding to KQ Pup A and B, which would allow us to determine RVs for both components, and thus also constrain the orbital parameters and mass ratio. The optical region of the spectrum is dominated by the RSG. Therefore, we determine the RV shifts of KQ Pup A using order-by-order cross-correlation of the optical spectra from STELLA (2024-2025) with a MARCS model<sup>8</sup> (Gustafsson et al. 2008) close in parameters to KQ Pup A, using the full wavelength range, but excluding Balmer regions. For KQ Pup B, we determine its approximate RV using lower Balmer emission lines, H $\alpha$  and H $\beta$ , which have the strongest emission features and best signal-to-noise compared to higher Balmer emission lines. Specifically, the RVs were determined based on the mirroring method (e.g., Arcos et al. 2018), i.e., by comparing direct and flipped Balmer emission profiles in *respefo*<sup>9</sup>. This method is commonly used for Be stars (e.g., Wolf et al. 2021; Harmanec et al. 2025).

Additionally, we also determine RV from the archival IUE spectra (1978-1995). We checked the wavelength calibration of the SWP observations by performing an interstellar medium (ISM) line alignment and removed these lines from the spectra. A co-added average spectrum was constructed as the template spectrum, and we then cross-correlated each observed spectrum with the template to obtain the cross-correlation functions (CCFs), using the full wavelength range, except for the spectrum edges. The RVs were then determined from the peak position of the calculated CCFs. In the SWP region, which is dominated by lines of the wind of the hot star, the determined RV corresponds to KQ Pup B, whereas in the IUE LWP region, which is dominated by lines forming in the ionized wind of the cool RSG, the determined velocity appears to track KQ Pup A.

In Fig. 4, we show the obtained high-cadence STELLA RV curve. We can see that the velocity of the KQ Pup A is increasing, following the periastron in January 2024, while the overall velocity of KQ Pup B (Balmer emissions) is decreasing, verifying that Balmer lines track the hot companion. Additionally, as shown in Fig. B.7, for the revised period of  $\sim 26$  yr determined by González-Riestra et al. (2002), our phased RV measurements agree very well with the archival RVs from Cowley (1965) taken during 1918-1964, validating the revised period. RVs determined from IUE spectra are used for orbital fit (see Sect. 3.6).

### 3.5. Astrometric orbit

We performed relative astrometry in order to determine the positions of the hot component KQ Pup B using the PMOIRE tool. In the near-IR interferometric VLTI dataset, the flux contribution of the hot component is too small to cause observable binary modulation; thus, the continuum would not be sufficient to determine the binary positions. Fortunately, relative astrometry was enabled by the detection of the hydrogen Bry line in our VLTI-GRAVITY data, which is the first time that this line could be used for a RSG binary system. This feature is very prominent in DPHI, suggesting a photocentre shift (see Fig. 5). The line is not so well visible in the flux, likely due to low resolution and other lines from the RSG.

For Be stars with disks, typical double-peaked hydrogen spectral lines are usually S-shaped in DPHI and V-shaped in VIS (e.g., Meilland et al. 2012), with point sources used to represent

<sup>8</sup> Downloaded from <https://marcs.oreme.org>.

<sup>9</sup> <https://astro.troja.mff.cuni.cz/projects/respefo/>

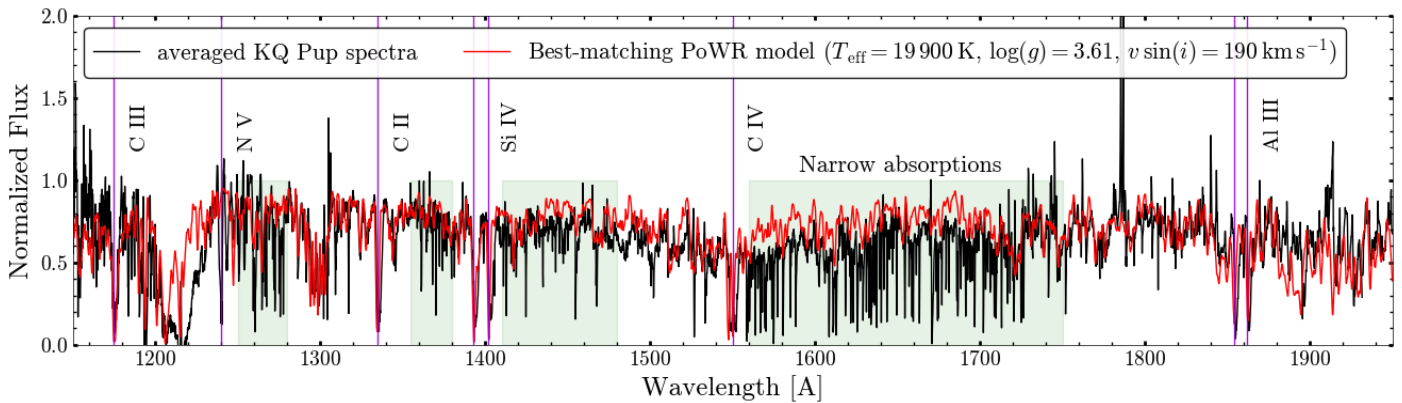


**Fig. 3.** Best-fit of PoWR model atmosphere to median IUE data of KQ Pup, showing full SWP range, for  $T_{\text{eff}} = 19.9$  kK. Main fitted lines of hot stars are shown (purple lines). Narrow lines (green background) are not reproduced by the high-rotating model and likely come from absorption in the RSG wind, see Fig. B.9. Detailed plots zoomed on specific features are available in Fig. B.4.

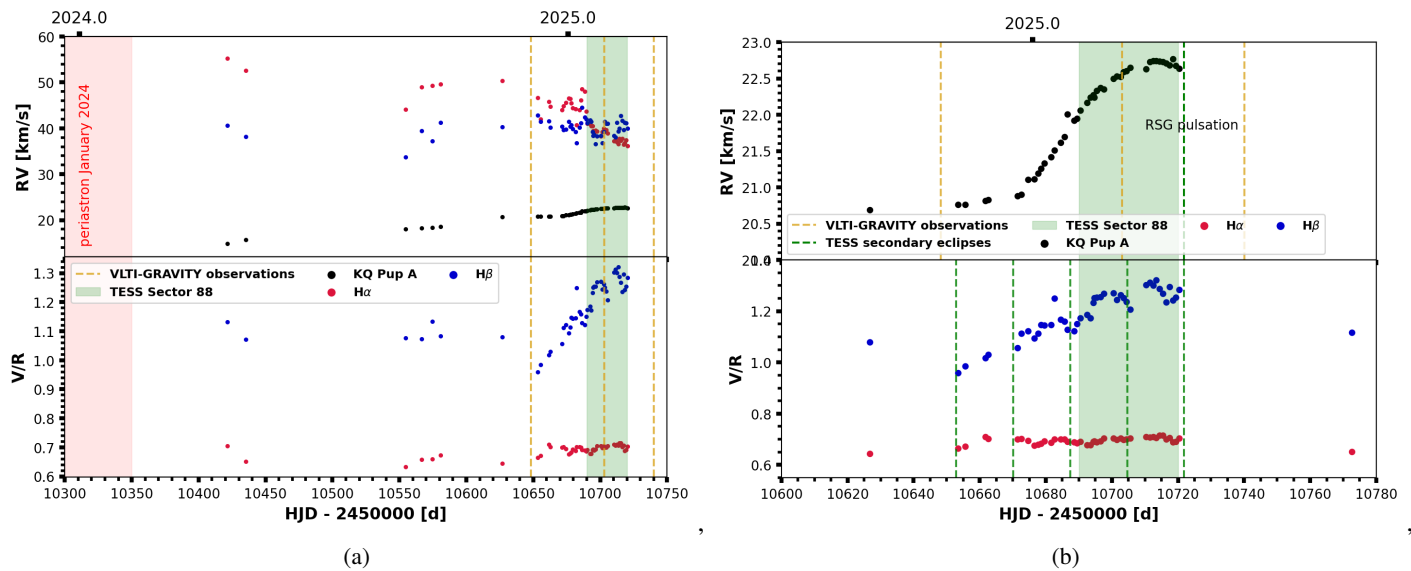


**Fig. 4.** Left panel: Determined RVs of KQ Pup A and B (based H $\alpha$  and H $\beta$ ) during the post-periastron epoch covered by STELLA. The vertical lines show the dates of VLTI-GRAVITY observations and TESS sector 88. Right panel: The same, but zoomed to the beginning of 2025. There is evidence for  $\sim 17$  d period variations in H $\beta$ , while longer trends due to the 26-year orbital period are also present. PLATOSpec spectrum taken in April 2025 is also included.

the stellar components (e.g., Frost et al. 2022; Klement et al. 2025). However, in our interferometric data, the Bry line has a shape of a single-component unresolved emission at all baselines. On the other hand, for a similar system,  $\zeta$  Aur, its transiting disk was imaged during its eclipse using interferometry (Kloppenborg et al. 2010, 2015). Furthermore, for VV Cep, when its B companion is eclipsed by the RSG, all higher Balmer lines and their emission disappear, while H $\alpha$  significantly weakens. Also, as shown for a similar system, WOH G64 by Munoz-Sanchez et al. (2024), Bry has the same profile as H $\alpha$ . Therefore, the association of Bry to the hot component is clear, and we assume that Bry feature represents the unresolved hot component KQ Pup B and/or its possible disk, which we cannot distinguish between, given the spatial frequencies probed by our observations.

Thus, we proceed to fit the Bry line in |V|, DPHI and T3PHI in PMOIRED using the unresolved point source model for KQ Pup B, while the rest of the spectrum is fitted with a uniform disk representing KQ Pup A. Based on  $a \sin(i)$  value from Rossi et al. (1992) and distance of 779 pc from BJ21, the semi-major

axis of the system is  $\sim 16$  mas, while KQ Pup B should be closer to KQ Pup A than that, following the recent periastron. We were able to recover the position of KQ Pup B via the Bry emission in all 3 VLTI snapshots, relative to the centre-of-mass. The best and most stable position solution gives a separation of about  $\sim 5$  mas, which we use. There are other local minima of the fit at  $> 15$  mas, which would result in unrealistic masses for the system. We show an example of the data and its fit in Fig. 5. We list the results from fitting in Table A.3, including the determined values of the angular diameter of KQ Pup A and the spectral parameters of Bry.

### 3.6. Global orbit fit

We fit the recovered positions of KQ Pup B with an astrometric orbit in PMOIRED. We do not fit well-known parameters -  $P$ ,  $K_A$ ,  $\gamma$ , and the time of periastron, while for other parameters, we use orbital parameters from Rossi et al. (1992) as start-

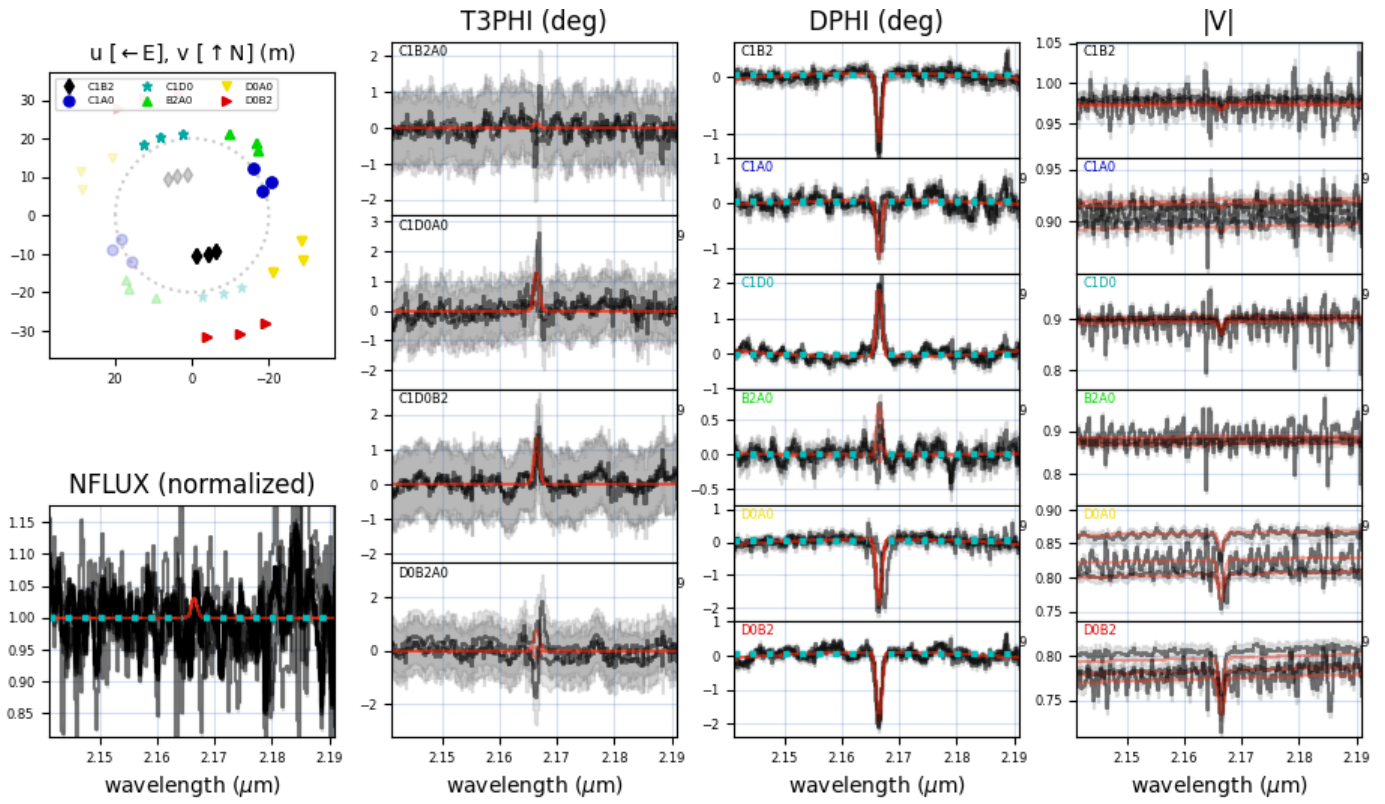


**Fig. 5.** PMOIRED fit of hydrogen Bry line for 3 VLTI epochs, red line shows the best fit in each epoch. UV coverage is shown in the left upper corner, and flux in the left bottom corner. In the remaining plots, the 3 main interferometric observables are shown - closure phase (T3PHI), differential phase (DPHI), and absolute visibility ( $|V|$ ).

ing values. We do the fitting in two ways. First, we fit only the VLTI data, including the RVs from the spectro-interferometric data. Second, we augment the fit with archival and new RV data (VLTI+RV) from other instruments, specifically for KQ Pup A (STELLA, Cowley 1965) and KQ Pup B (Bry with VLTI, H $\alpha$  with STELLA, and IUE SWP). To ensure that the orbital solution is not affected by intrinsic variability in our targets, we set RV errors for the fitting based on observed variability in Fig. 4a, i.e., we set the velocity error for KQ Pup A to  $2.5 \text{ km s}^{-1}$  (RSG oscillations) and to  $5 \text{ km s}^{-1}$  for KQ Pup B (variability of Balmer lines).

In Fig. 6, we show our best orbital fit of the recovered Bry positions, and in Table 1, we list the resulting orbital parameters. In both variations of the fitting, we obtain similar results, demonstrating that a few VLTI snapshots can give a reasonable result, although including the RV from other parts of the orbit improves the fit. Our obtained parameters are relatively similar to Rossi et al. (1992), but in this work, we obtained for the first time inclination  $i$ , longitude of the ascending node  $\Omega$ , and projected semimajor axis  $a \sin(i)$ . The astrometric solution itself would be sufficient to determine the semi-major axis  $a$ , and thus the total mass of the system, if the distance is well-known. Nonetheless, combining this with the RV of both components, we can also find the parallax of the KQ Pup system. From a global fit to all data, we find  $\pi = 1.29_{\pm 0.10} \text{ mas}$ , which is consistent within uncertainties with the parallax obtained by Gaia (BJ21). We also find a high mass ratio of  $q \sim 1.5$ . Such a high mass ratio is not expected, as it would suggest that the less evolved B-type companion is more massive than the RSG component. We explore possible scenarios in Sect. 4.

High-precision astrometry revealed KQ Pup B as it leaves the periastron, moving by about 3 mas toward the NW direction between December 2024 to March 2025. In relative astrometry, the primary star is assumed to be at the centre of mass. However, considering the mass ratio, we know that at the time of VLTI observations, it would be at a similar distance from the centre of mass as KQ Pup B, but on the opposite side, moving toward SE. Considering the determined average angular diameter of KQ Pup A of  $\sim 5.87 \text{ mas}$ , i.e.,  $R_A = 491_{-36}^{+41} R_\odot$  (based on the determined  $\pi$ ), there would be a separation of several RSG radii between the components. Based on the RV difference between the A and B components, B is moving supersonically through the wind of the RSG near the periastron and likely also for a large part of the orbit (considering the typical sound velocity of  $v_{\text{sound}} = 5 - 15 \text{ km s}^{-1}$ , see Appendix D.2).

#### 4. Discovery of KQ Puppis Bb

We investigated TESS data for the KQ Pup system and discovered that this system exhibits clear primary and secondary eclipses in all 4 sectors covered with TESS between 2019-2025, with a period of about  $P = 17.2596 \text{ d}$  and the secondary eclipse not occurring in the middle of the period; therefore, the related orbit is eccentric. In Fig. C.1, we show raw TESS data for KQ Pup, and in Fig. 8, we show clean phased normalized data. The TESS light curves were detrended using the Chebyshev polynomials. Each sector was divided into smaller parts to better cover the trend influence and fitted by a polynomial of degree  $n$  between 5 and 10. We verified that there are no near-eclipsing binaries (EBs) with a similar period, and we also verified the validity

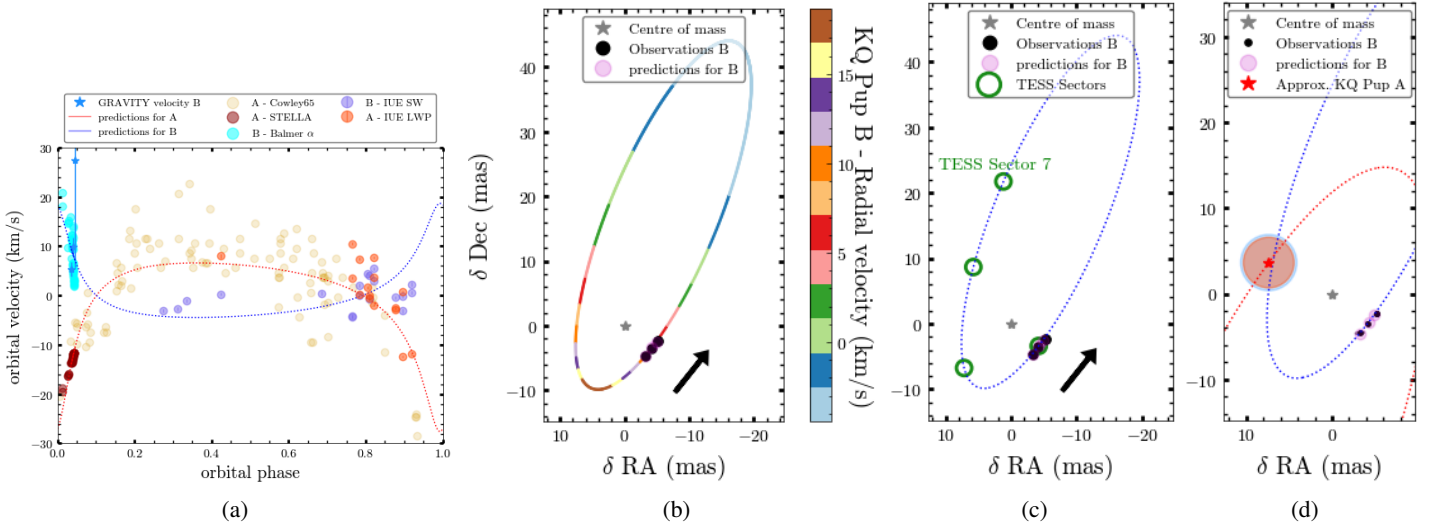


**Fig. 6.** Astrometric orbit for KQ Pup system. *Panel a)*: Phased RV, including the archival data. *Panel b)*: Fitted orbit of KQ Pup B, using the Bry emission feature. Colored based on RV for KQ Pup B in the first plot. *Panel c)*: Fitted orbit of KQ Pup B, but showing only the recovered positions, including the direction of motion, as well as approximate locations of TESS Sectors. *Panel d)*: The same, but showing the approximate location of KQ Pup A during the time of our VLTI observations. We strongly emphasize that in relative astrometry, we do not measure the position of the primary star. Therefore, this last panel is just a sketch of the system, based on other properties derived. We note that the shown astrometric solution is based on VLTI only.

of the association of the light curve to the KQ Pup system using Target Pixel Files (TPF).

We also investigated the  $O-C$  values of the eclipse timings in TESS data to investigate whether we could measure a light travel time due to the orbital motion of KQ Pup Ba+Bb. The  $O-C$  residuals suggest that during and after the periastron, the eclipses occur later than in the previous sectors. This would agree with the orbit presented in Fig. 6 and with parameters listed in Table 1, because for roughly half of the orbit, closer to the periastron, Ba+Bb are accelerating away from us and are farther from us. The last two sectors also have much more noise and other activity compared to the first two sectors (see Fig. C.1), which would agree with Ba+Bb entering denser wind of the RSG, as it gets closer orbital path of KQ Pup A. But further TESS observations along the orbit would be needed to build an  $O-C$  curve which would be able to fully constrain the light-time effect in the system.

Considering the short orbital period, this third component would not fit in the orbit around the RSG KQ Pup A. The shortest known or suspected companions of RSGs have periods of at least several years (e.g., Patrick & Negueruela 2024). From Kepler's third law, a period of the order of several weeks would result in an orbit of several  $\sim 10 R_\odot$ , i.e., inside the RSG. Therefore, we investigate the association of the eclipsing binary with KQ Pup B, the previously assumed single hot companion. This scenario is more likely as there are several known short-period massive early B-type binaries, with the shortest periods of the order of days (e.g., Labadie-Bartz et al. 2022; Sharma et al. 2022).

We investigated V/R ratios of Balmer lines in our high-cadence STELLA spectra (2024-2025). A companion passing through or near the disk can inflict V/R variations of a similar timescale as the orbital period (Rivinius & Klement 2024). This was also shown in recent detailed simulations of Be + companion in the disk modelling by Rubio et al. (2025). In Fig. 4b, we can see that the V/R variations appear to be phased with the TESS eclipses of  $P = 17.2596$  d, especially for H $\beta$  variations. Period analysis for H $\alpha$  and H $\beta$  revealed several periods close to

$\sim 17$  d. There is also a very strong trend of about  $\sim 90$  d (apart from a longer trend due to the 26-yr orbital period), which is quite similar in timescale to the RSG pulsation at the beginning of 2025.

Next, in Fig. 6d, we investigate short-term variations of the recovered positions of KQ Pup B from VLTI. As we discussed in Sect. 3.5, Bry emission is either associated with (one of) the hot components (Ba, Bb) or the disk. Even in the case of the disk, the position variations could still correspond to KQ Pup Bb, as demonstrated in simulations by Rubio et al. (2025), where the strongest Bry emission can arise from part of the disk disturbed or accreted by the companion. The differences between predicted orbit and measured Bry position lie at the edge of the ellipse error bars, i.e., between  $\sim 0.1 - 0.3$  mas in different VLTI observations. Assuming  $M_{Ba+Bb} \sim 14 M_\odot$  as found in the previous Section, the resulting semi-major axis would be  $a_{Ba+Bb} \sim 0.3$  au, i.e.,  $\sim 0.4$  mas. Considering that our VLTI observations are taken at similar phases of  $P_{Ba+Bb}$  (within  $\sim 0.33$  phase difference from each other), the recovered position variations of Bry are compatible with the existence of the Ba+Bb system, which could be oriented along the A+B orbital path. However, more VLTI-GRAVITY observations will be necessary to precisely measure the astrometric orbit of Ba+Bb, especially those at longer baselines, i.e., higher spatial resolution. Such observations could also help to resolve the source of Bry emission. We also emphasize that RSG+B binaries in the VLTI-GRAVITY sample normally do not show Bry feature, inferring that in this case, we detect it because of an unusual increased flux contribution, likely from the disk emission.

We also further investigate the archival IUE UV spectra to better characterize KQ Pup Bb. RVs determined from IUE (Fig. 6a) do not show large departures from the expected orbital velocity, up to  $\pm 10$  km s $^{-1}$ . That, along with  $i \sim 90$  deg (TESS eclipses), would imply a high mass ratio, i.e.,  $M_{Ba} \gg M_{Bb}$ . In Sect. 3.3, we were able to fit the IUE spectra with a single hot component, reproducing the majority of the spectral features. Some spectral features (e.g., N V) were not reproduced so well

**Table 1.** Best-fit orbital parameters of KQ Pup A and Ba+Bb based on VLTI astrometry and archival RVs, while we also list properties derived from asteroseismology and model atmospheres.

Astrometric solution for KQ Pup system		
	VLTI only	VLTI global + RV
$P$ [d]	9500	
$MJD_{\text{periastron}}$ [d]	60310	
$\gamma$ [km s $^{-1}$ ]	34.4	
$K_A$ [km s $^{-1}$ ]	17.1	
$e$	$0.64_{\pm 0.03}$	$0.62_{\pm 0.01}$
$\omega$ [ $^{\circ}$ ]	$194.86_{\pm 4.43}$	$203.48_{\pm 2.17}$
$\Omega$ [ $^{\circ}$ ]	$334.95_{\pm 6.47}$	$319.25_{\pm 3.61}$
$i$ [ $^{\circ}$ ]	$68.46_{\pm 2.96}$	$70.28_{\pm 1.24}$
$a \sin(i)$ [mas]	$29.38_{\pm 3.77}$	$30.21_{\pm 1.80}$
$q$	-*	$1.50_{\pm 0.16}$
$\pi$ [mas]	-**	$1.29_{\pm 0.10}$
$a$ [au]	$24.61_{\pm 3.16}$	$24.89_{\pm 1.48}$
$M_A$ [ $M_{\odot}$ ]	$8.89_{-3.00}^{+3.88}$	$9.12_{-1.53}^{+1.73}$
$M_{\text{Ba+Bb}}$ [ $M_{\odot}$ ]	$13.14_{-4.44}^{+5.74}$	$13.68_{-2.30}^{+2.59}$

\* not fitted, using the value from the global fit

\*\* not fitted, BJ21 distance is used to calculate  $a$

## Other results

Asteroseismology	Model atmosphere	
	KQ Pup A	KQ Pup B
$T_{\text{eff}}$ [K]	$3660_{\pm 170}^{*}$	19 900
$\log(L)$ [ $L_{\odot}$ ]	4.55-4.77*	$3.95_{\pm 0.4}$
$M$ [ $M_{\odot}$ ]	7.1-11.8	20 000
Interferometry		
$R_A$ [ $R_{\odot}$ ]	$491_{-36}^{+41}$	$v \sin i$ [km s $^{-1}$ ]
$\log(L_A)$ [ $L_{\odot}$ ]	$4.58_{-0.06}^{+0.08}$	$190_{-70}^{+70}$
Evolutionary models		
age [Myr]	18.7-46.9	$v_{\infty}$ [km s $^{-1}$ ]
$M_{\text{Ba}}$ [ $M_{\odot}$ ]	$\sim 7.5$ -11.5	$v_{\text{turb}}$ [km s $^{-1}$ ]
$M_{\text{Bb}}$ [ $M_{\odot}$ ]	$\sim 1.2$ -8.1	$\log \dot{M}$ [ $M_{\odot} \text{ yr}^{-1}$ ]
		$X_H$
		$\xi_{\text{phot}}$ [km s $^{-1}$ ]
		$\xi_{\text{max}}$ [km s $^{-1}$ ]

\* from Rossi et al. (1992) and Healy et al. (2024)

\*\* cut at 200 km s $^{-1}$

and could imply a higher  $T_{\text{eff}}$  than 20 000 for the Bb component (but could also be reproduced by X-rays). We also search for other features that could correspond to KQ Pup Bb. No secondary peak was found in the cross-correlation function, even when different regions in the IUE spectra were cross-correlated separately. A few narrow lines appear to exhibit larger velocity variations than KQ Pup Ba on timescales much shorter than  $P_{\text{AB}}$  (see Sect. 4.3 for more discussion on Ba+Bb orbit). However, upon comparing the IUE spectra of KQ Pup to Betelgeuse, which has no known massive B-type companion, it is apparent that the majority of these lines form in the cool wind of the RSG (see Fig. B.9). To be able to measure and identify lines belonging to KQ Pup Bb, and thus to reliably characterize Ba+Bb or-

bital parameters, it will be necessary to obtain new high-cadence high-resolution UV spectra.

Overall, the existence of KQ Pup Bb is strongly implied by the obtained mass ratio  $q_{\text{AB}} \sim 1.5$ , which gives higher mass to the Ba+Bb pair. If KQ Pup B were a single star with a larger initial mass than the RSG, it would already be more evolved than the RSG. Therefore, either  $M_A \gtrsim M_{\text{Ba}}$ , with the remaining mass in Bb, or there has been significant mass transfer in the system. Mass transfer between Ba and Bb could be supported by a possible high mass ratio between Ba and Bb (from low velocity spread of Ba), which is common for Be+sdOB systems (e.g., Lechien et al. 2025). However, at lower wavelengths, we have not detected any He II lines, nor strong He I lines, which are common for hot stripped subdwarfs. Likewise, the orbit of KQ Pup A and the inner binary Ba+Bb is wide enough to prevent a  $\sim 9 M_{\odot}$  star from filling its Roche-lobe. This is true even when considering that the Roche-lobe radius at periastron is smaller, at around  $700 R_{\odot}$  (using the formula from Eggleton 1983 with the orbital separation replaced by the periastron distance), while RSG models of  $M_i = 8 - 12 M_{\odot}$  do not typically extend above  $\sim 500 R_{\odot}$  (e.g., Choi et al. 2016), which is also in agreement with our radius for KQ Pup determined from interferometry (see Table 1).

Furthermore, previous studies showed that mass transferring tertiaries are rare and in many cases drive the inner binary to undergo mass-transfer first, or even merge (de Vries et al. 2014; Toonen et al. 2020). In the absence of other evidence of past mass transfer between the outer tertiary and the inner binary, as well as between the inner binary components, we will work under the assumption that we are observing the system before having undergone any significant mass transfer, apart from wind-accretion.

### 4.1. Wind Roche Lobe Overflow

We see strong signatures of a disk (Balmer and Brackett emission) in our data, which could imply mass transfer. This could be reconciled with our results if the disk is fueled by wind Roche-lobe overflow (wind-RLOF, Mohamed & Podsiadlowski 2007), i.e., by accretion from the dense RSG wind, and not by mass transfer between Ba+Bb. Indeed, we see that Balmer emissions strongly depend on the AB orbit, with the strongest emission components at periastron and then nearly disappearing by apastron (see Sect. 3.2). Meanwhile, the VR peak separation at apastron is half of the value at periastron, suggesting that the properties of the disk change significantly, possibly having a different size or mass. For eccentric accreting systems, significant changes along the AB orbit would be expected (Okazaki 2007; Lajoie & Sills 2011; Saladino & Pols 2019). The wind-RLOF scenario is further supported by V/R variations showing a strong trend close in timescale to the RSG pulsations,  $\sim 90$  d (see Fig. 4b). If the disk is accreting directly from the RSG wind, the accretion rate (and hence also disk properties) would be expected to vary on a similar timescale, while the disk is also perturbed by Bb on  $\sim 17$  d timescale, as also shown by V/R variations.

Such a scenario can also be aided by the presence of the extended envelope on top of KQ Pup A. RSGs are known to show extended molecular layers (e.g., Arroyo-Torres et al. 2015; González-Torà et al. 2024) that may reach up to several stellar radii  $R_{\star}$ . Consistently, our VLTI data of KQ Pup A indicate that the CO molecular envelope is extended by  $\sim 1.13 R_{\star}$  in near-IR (see Appendix A). Compared to other sources with similar CO extension by González-Torà et al. (2024) and considering that the star shows IR excess (e.g., Cruzalèbes et al. 2019), this indi-

cates a possible extension at mid-IR wavelengths of up to about  $\sim 10 R_\star$ . With simple theoretical calculations regarding the density structure in the wind and accretion rate on the inner binary (see Appendix D.2), we also conclude that the accretion rate of material on the inner binary is about  $< 10\%$  of the mass-loss rate from KQ Pup A, and is driven by wind-RLOF. Given the short lifespan of KQ Pup A as a RSG, this mass accretion of its wind has negligible consequences in terms of the mass budget of the hot components. If KQ Pup A does reach core-collapse, which is likely given the mass estimate, this extended envelope may provide flash-ionization features in the supernova at early times (Ercolino et al. 2024).

#### 4.2. Constraints from stellar evolutionary models

Considering the previously determined masses, no evidence of significant mass transfer, and the similar depth of primary and secondary eclipses in TESS, it is likely that Bb is also a main-sequence star. To test whether Ba and Bb could still be a pair of main-sequence stars by the time KQ Pup A develops into a RSG, we employed the publicly available MESA evolutionary models (Paxton et al. 2011, 2013, 2015) from the MIST database (MESA Isochrones and Stellar Tracks, Dotter 2016; Choi et al. 2016), see Appendix D.1 for details. Using the observed mass of KQ Pup A (Table 1) and the fact that it appears as a RSG, we obtain an age constraint of 18.7 – 46.9 Myr (see Fig. D.1). Assuming that all three stars are co-eval, and that Ba and Bb have not yet exchanged mass via Roche Lobe overflow, with  $M_{\text{Ba}} > M_{\text{Bb}}$ , we obtain the mass-constraints of  $5.7 \lesssim M_{\text{Ba}}/M_\odot \lesssim 11.7$  and  $1.2 < M_{\text{Bb}}/M_\odot \lesssim 8.1 M_\odot$  (see Appendix D.1), with the lower limit of  $1.2 M_\odot$  based on the minimum mass of Bb necessary to reach the main sequence within the age constraint. Therefore, KQ Pup Bb is likely an early A/F main-sequence star.

Based on numerous determined physical parameters for KQ Pup A and Ba, we further tested whether they are indeed co-eval stars and whether we could estimate more of their properties from evolutionary tracks. We thus compared their Hertzsprung–Russell diagram (HRD) positions to isochrones from MIST (Dotter 2016), selecting models with solar composition ( $[\text{Fe}/\text{H}] = 0$ ), and rotation enabled ( $v_{\text{init}}/v_{\text{crit}} = 0.4$ , based on our  $v \sin i$  value). We used the online interpolator<sup>10</sup> to calculate isochrones at the age limits (18.7 and 46.9 Myr) and at a few intermediate values, see Fig. 7.

As shown in Fig. 7, star A is at the RSG branch, at, but more likely above the blue loops that indicate the He-core burning phase. We note that we are not overly concerned by the offset of star A from the models: as Joyce et al. (2020) showed, changes to various model parameters, especially the mixing length and mass loss, can induce shifts up to  $\pm 200$  K in high-mass RSG models. Initial masses for models around the position of A are between  $9$ – $12 M_\odot$ , while the present-day mass of the RSG could be lower by up to  $\lesssim 0.5 M_\odot$  (see Appendix D.1).

The other well-constrained star, Ba, appears to lie close to the main sequence. We highlight the terminal-age main sequence (TAMS) model points with red dots: the star is very close to them, indicating that it is nearing, or just past the end of its main-sequence lifetime. Based on the luminosity uncertainties for Ba, we estimate an age range of  $26 \pm 7$  Myr for the system. Indeed the position of Ba (Fig. 7) fits well between the isochrones at 19 and 33 Myr, and the mass-constraints that arise ( $11.0$ – $11.5 M_\odot$  and  $7.5$ – $8.5 M_\odot$  from each isochrone respectively) is also well within the values inferred just from the constraints in age

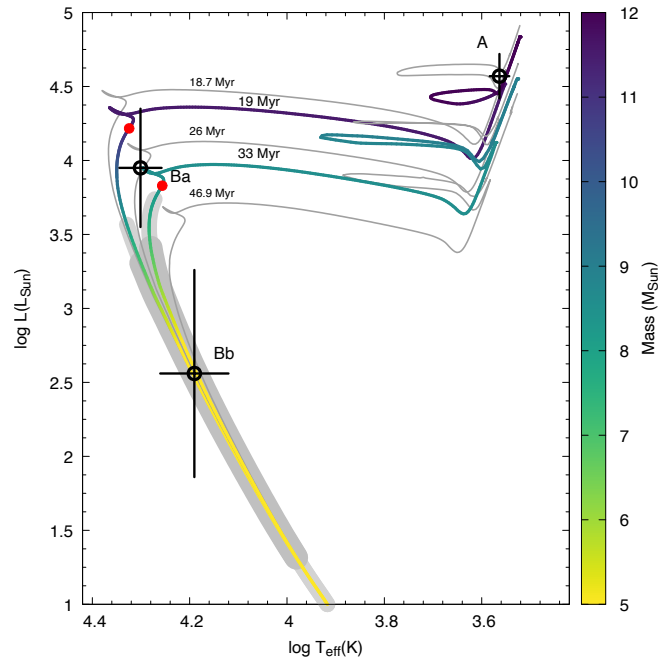


**Fig. 7.** Positions of KQ Pup A and Ba on the HRD, compared to isochrones interpolated from the MIST database. Red dots indicate the terminal-age main sequence (TAMS) evolutionary points. The thick grey area shows the range of models that fit the mass constraints for Bb, with the area of the most likely mass at  $4.4 M_\odot$  highlighted with the large cross. Grey lines indicate the age limits and the middle value from evolutionary models.

and masses. Mass ranges for A and Ba along the isochrones are thus in good agreement with other mass inferences, and their positions are compatible with co-eval evolution. This agrees with RSG+B systems studied by Patrick et al. (2025), where the majority of their systems could also be explained by co-eval evolution.

It is much harder to constrain Bb on the isochrones, since at the moment we can only infer its mass from the difference between the combined mass of the B components and the inferred mass for Ba. Given the large uncertainties, the possible values for Bb span between masses  $1.2$ – $8.1 M_\odot$  (based on the evolutionary tracks) or  $2.1$ – $7.0 M_\odot$  (based on the astrometric mass range for Ba+Bb). Thus, we highlight the ranges defined by these two limits for Bb with thinner (wide range) and thicker (narrow range) grey areas in Fig. 7. We note that the plot only extends to  $\log L = 1.0$  in order to highlight the differences between the post-MS branches, but the models only reach the lowest mass and the ZAMS point at  $\log(L) \approx 0.23$ . We also include a fiducial point with large error bars around  $4.4 M_\odot$ , the most likely mass range for Bb based on the mean dynamical masses.

#### 4.3. Orbital modeling of KQ Pup Ba+Bb

We calculated some representative binary models with the PHOEBE code to simulate the Ba+Bb pair (Prša et al. 2016; Conroy et al. 2020). We used the physical constraints presented in this work, plus the phase differences between the primary and secondary eclipses in the TESS light curve.

Based on the luminosity estimates, we first calculated the brightnesses of the stars in the TESS passband to deblend the light curve from the contribution of KQ Pup A, and to esti-

<sup>10</sup> [https://waps.cfa.harvard.edu/MIST/interp\\_isos.html](https://waps.cfa.harvard.edu/MIST/interp_isos.html)

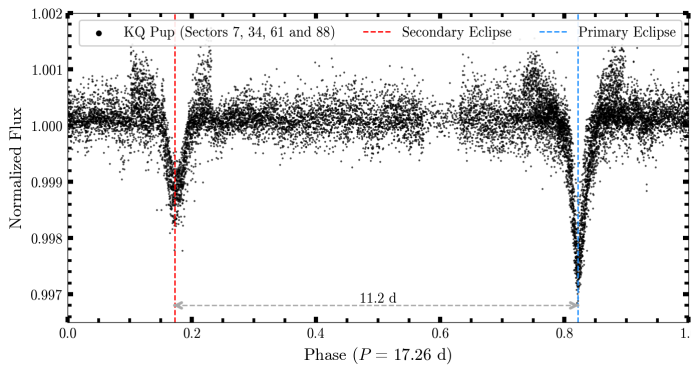


**Fig. 8.** Cleaned and normalized TESS-SPOC data, phased by the period of eclipses  $P = 17.2596$  d, which corresponds to Ba+Bb orbit and shows an eccentric orbit. Each sector is shown in Fig. C.1.

mate the true eclipse depths. Since the TESS passband is very similar to the *Gaia*  $G_{\text{RP}}$  passband, we used the bolometric correction (BC) tables published by Jordi et al. (2010). The  $BC_{\text{RP}}$  values change quite rapidly around the physical parameters of both A and Ba, but we estimate that for A,  $BC_{\text{RP}}$  is between  $-0.2$  and  $0.5$  mag, while for Ba it is between  $-2.3$  and  $-2.9$  mag. From these we estimated the absolute magnitudes and the flux ratios, and found that the dilution factor (the ratio of the combined flux of the system relative to the flux level of Ba+Bb) is between  $12\text{--}55$  or  $22\text{--}70$ , for  $\log L_A = 4.55$  or  $\log L_A = 4.77$ , respectively. With these dilution factors, we estimate that the true eclipse depth of Ba+Bb is in the range of  $0.02$  to  $0.20$  mag.

The RV data is unsuitable to fit the orientation of the orbit properly at this point. Observations are scattered over a long period of time, and thus are affected by both the light-time effect and potential dynamical effects from the A+B orbit, as well as by the accumulation of uncertainties over hundreds of Ba+Bb orbits. We estimate an RV amplitude limit of  $A_{\text{RV}} < 10$  km s $^{-1}$  based on the scatter of the B velocity data. We note that for eccentric orbits, stars might spend most of the orbit at low velocities, with the RV spiking only around pericenter - similarly to the orbit of A+B. A few lines indicate possible RV signals up to  $50$  km s $^{-1}$  (see Fig. B.5), highlighting the possibility of higher velocities at narrow phase intervals.

Nevertheless, we can still estimate the minimum eccentricity of the pair. The offset of the secondary eclipse from the 0.5 phase between primary eclipses clearly indicates a significantly eccentric orbit for Ba+Bb. Assuming an orbit where the semimajor axis is perpendicular to the line of sight, eclipses happen  $90^\circ$  apart from pericenter. This is the shortest and fastest arc a star can take around another between eclipses, so the differences between the eclipse phases can constrain the minimum eccentricity necessary.

We therefore decided to model the orbit in PHOEBE with the semimajor axis fixed to be perpendicular to the line of sight, and the eclipses being central ( $i = 90^\circ$ ). We chose four mass values for Ba based on the isochrone points near the location of Ba in Fig. 7:  $8.3$ ,  $8.9$ ,  $9.4$ , and  $9.9 M_\odot$ . We then selected a few test points for Bb, at luminosities  $\log(L) = 2$ ,  $2.5$ , and  $3.0$ , as well as two low-mass test points at  $1.5$  and  $2.0 M_\odot$ .

The preliminary PHOEBE models are presented in Fig. 9, where we colored the selected model combinations according to the Bb/Ba mass ratio. The RV curves suggest that a low-mass Bb component ( $< 2 M_\odot$ ) would be in good agreement with the RV limits we estimated. We calculate the minimum eccentric-

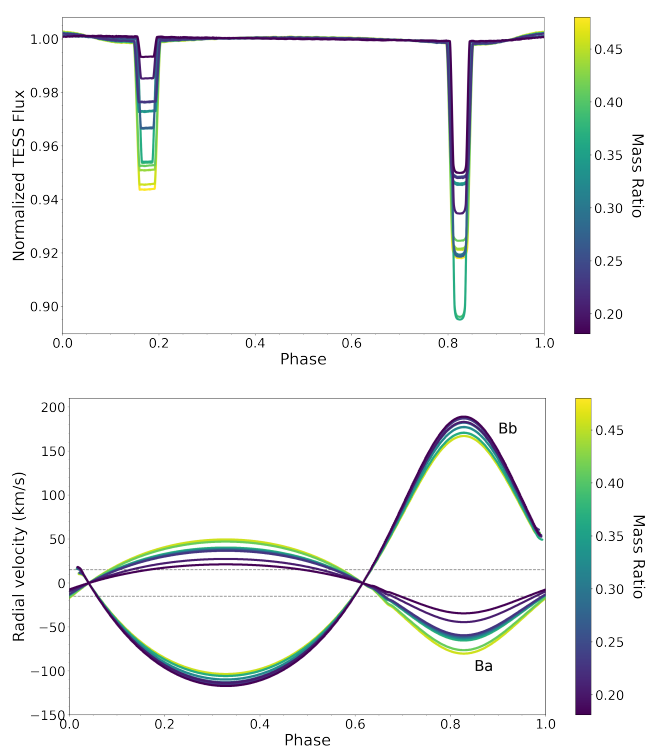


**Fig. 9.** Preliminary PHOEBE models for the Ba+Bb pair. *Upper panel*: light curves in the TESS passband. *Lower panel*: RV curves for both components. The color axis indicates the mass ratio of the two stars. Grey lines indicate the  $\pm 10$  km/s velocity amplitude limit (based on observed velocity scatter for Ba). We note that in our spectra, no clear signatures of Bb were found; therefore, its velocity is not measured.

ity of the orbit to be  $e_{\text{Ba+Bb},\text{min}} \geq 0.236$ . The eccentricity of the inner-binary can be caused by the eccentric Kozai-Lidov effect (Kozai 1962; Lidov 1962; Naoz et al. 2013) as well as the angular-momentum exchanges with the wind accreted from KQ Pup A.

The light curves in the upper panel of Fig. 9 show flat-bottomed eclipses, which are clearly different from the observed, V-shaped eclipses in Fig. 8. Furthermore, central eclipses, or eclipses with the same impact parameter, would make the differences between eclipse depths more pronounced than what we see in the observations. The TESS light curve, therefore, suggests that the impact parameters for the two eclipses may be different, and that both eclipses are partial or grazing, suggesting an inclination slightly offset from  $90^\circ$ .

## 5. Other triple candidates

Following our discovery, we also cross-check the list of 651 Galactic RSGs (and RSG candidates) by Healy et al. (2024) with the TESS catalogue, and look for eclipses in RSG systems. At first, we find about 12 candidates. Similar to KQ Pup, we first verify that there are no blends with near-EBs within 5 arcmin, and we also check the TPF files to validate the eclipses. We identify half of the initial candidates as likely blends with near-EBs. Thus, we are left with a sample of about half a dozen additional likely candidates, where almost all are known or suspected RSG+B binaries, which further validates the final sample, as such short-period eclipses could not occur for single RSGs. TESS data for the promising candidates are shown in Fig. C.2

and listed in Table 2. We also took new PLATOSpec spectra for the promising candidates to check the binary spectral properties, as shown in Fig. B.8.

We note that 4 targets from our sample were part of the TESS Eclipsing Binary stars catalogue (Prša et al. 2022), consisting of several thousand candidates identified with an automatic algorithm. KQ Pup was also part of the list, but with incorrect ephemerids and period. For the other 3 stars in their sample, HD 300933, V340 Sge, and V349 Car, there is a similar period as we found. Furthermore, two of our candidates, AZ Cas and V1092 Cen, are also included in Dorn-Wallenstein et al. (2020), where they studied the stochastic variability in selected evolved supergiants with TESS, but did not discuss any eclipses. All our other candidates show much shorter eclipse periods than KQ Pup. Such periods are common in the literature. For example, there are several papers that report on eclipses of hot stars in TESS, including their variability, such as for B stars (e.g., Sharma et al. 2022), as well as for Be stars (e.g., Labadie-Bartz et al. 2022).

### 5.1. Notes on individual targets

Below, we report some additional notes on individual targets.

- FR Sct and HD 303344 - these candidates shows semi-detached eclipses, making them the most interesting targets for future observations. FR Sct was also part of the initial list of 13 VV Cephei stars by Cowley (1969). Pigulski & Michalska (2007) reported likely photometric eclipses of  $P = 3.53$  d but this target was never followed up or confirmed. Considering that eclipses of FR Sct were detected with ASAS, that would also make it the most accessible target for ground-based photometry.
- AZ Cas - this star is also a well-known VV Cephei star; it was part of the initial sample of 13 stars (Cowley 1969). The orbital period is  $\sim 9.3$  yr and it undergoes full eclipses, with a totality lasting about  $\sim 100$  d (AAVSO). Based on our reported TESS eclipses, AZ Cas would become the first known RSG system showing both inner and outer eclipses, if confirmed.
- VV Cep - the most famous star of the VV Cephei sample. This star experiences full eclipses (e.g., AAVSO), with the totality lasting about  $\sim 450$  d. Pollmann & Bennett (2020) reported strong V/R variations of about  $\sim 42$  d, including during the totality, while there are also V/R variations related to its 20.36 yr orbital period. Therefore, as in our case, the shorter V/R variations could correspond to a hypothetical VV Cep Bb.
- Wide systems - there are some systems with large angular separation between the RSG and their companions, i.e., similar to the Antares system ( $\sim 5$  arcsec between Antares A and B) or even larger. Eclipses detected for such companions are difficult to separate from blends with nearby unrelated EBs. In the case of a promising candidate V340 Sge, it has a wide companion at  $\sim 30$  arcsec (Dommangé & Nys 2002), showing the same eclipses, while a discarded candidate BD+532693 is surrounded by 4 B-type stars (2 of them Be-type) within  $\sim 35$  arcsec, one of them showing the same eclipses. To judge whether such wide systems are physically associated and thus to confirm whether such systems are wide hierarchical triple systems, would be beyond the scope of this paper, and it will become clearer with the release of upcoming epoch astrometry in Gaia DR4.

## 6. Discussion

### 6.1. Classification of RSG binaries

In the community, there is confusion about the classification of binary RSGs. Pantaleoni González et al. (2020) compiled a sample of about 100 Galactic RSG binaries based on spectral type, several of which may actually not be RSGs from an evolutionary point of view. Indeed, the more recent list by Healy et al. (2024) gives a smaller number. Meanwhile, Munari et al. (2021) selected M supergiants from the sample by Pantaleoni González et al. (2020), considering them all as VV Cephei type. However, in the new large samples of RSG+B binaries in the Local Group Neugent et al. (2019); Patrick et al. (2022, 2025), the majority of their binaries were not reported as interacting, except for 4 companions embedded in the RSG wind by Patrick et al. (2025). Neugent et al. (2019) also reported that one of the systems in the sample is the first known RSG+Be pair, based on Balmer emission lines. However, we note that all the previously known VV Cephei RSGs (Cowley 1969) also show Balmer emission lines, as previously discussed, and were sometimes also considered to host a Be companion, including for KQ Pup (Altamore et al. 1992). RSG binaries were also sometimes confused with  $\zeta$  Aurigae group, which consists mostly of earlier and less massive red giants, except for VV Cep star. Historically, some of the VV Cephei stars were also misclassified as classical symbiotic stars, i.e., systems consisting of an evolved red giant and white dwarf (e.g., Merc et al. 2019). Nonetheless, VV Cephei type binaries could likely also be classified as symbiotic B[e]-type (symB[e]) stars (Lamers et al. 1998; Munoz-Sánchez et al. 2024), interacting symbiotic systems consisting of a cool (super)giant and a hot component, enshrouded in a nebula producing forbidden emission lines.

We took new PLATOSpec spectra for the promising candidates in our TESS sample (Fig. B.8). We confirm the VV Cephei properties of AZ Cas and FR Sct. For other RSG+B binaries in our sample, there are no Balmer emission features. We note that the same is the case for the majority of RSG+B binaries, based on archival spectra as well as our new spectro-interferometric survey (a spectral atlas for southern RSG binaries shall be published in a forthcoming study).

### 6.2. Classification of hot components in VV Cephei systems

To find out whether the KQ Pup Ba+Bb system could correspond to some of the known classes of short-period massive binaries, we compare the available spectra. A natural candidate for comparison would Be+sdOB binaries, which are also routinely studied using Bry hydrogen line (Klement et al. 2024, 2025). However, we have not found any typical spectral features of such hot stripped He-rich subdwarfs in UV, nor in the optical spectrum. Although it is also possible that, since the hot companions are embedded in very dense CSM, we simply cannot see the lines, therefore, the stripped scenario is not fully ruled out. In any case, our systems could be younger than typical Be+sdOB binaries (e.g., Wang et al. 2021; Lechien et al. 2025), therefore, a significant mass transfer may not have occurred yet, considering that the RSG component has not exploded as SN yet.

In the UV region, we find more similarities with B[e] supergiants. For example, GG Car shows quite a similar IUE spectrum, while it has other similar properties - an eclipsing companion at about  $\sim 30$  d, a disk, and dense CSM (Gosset et al. 1985; Marchiano et al. 2012; Kraus et al. 2013; Porter et al. 2021, 2022; Kashi 2023). However, the evolutionary status of B[e]sg

**Table 2.** List of other promising and discarded hierarchical triple candidates from TESS, with spectral binary signatures listed based on our newly taken PLATOSpec spectra (Fig. B.8) or archival spectra, when available.

Confirmed TESS candidates						
Star	Spectral type	Period [d]	H em.	[Fe II] em.	Multi-core Na I	Notes
KQ Pup	M2Iab+B0V	17.26	✓	✓	✓	VV Cep type
Promising TESS candidates						
Star	Spectral type	Period [d]	H em.	[Fe II] em.	Multi-core Na I	Notes
AZ Cas	K5Iab+B	1.25	✓	✓	✓	VV Cep type, irregular ecl.
HD 300933	M3Iab+B2V	2.91	X	X	✓	binary RSG
HD 303344	M2Ib+B	2.59				binary RSG
FR Sct	M0+B	3.53	✓	✓	✓	VV Cep type
V340 Sge	K4Ib(+A)*	1.63	X	weak	broad	single RSG?
Discarded TESS candidates due to a likely blend with near-eclipsing binaries of similar periods or due to signal offset						
Star	Spectral type	Period [d]	H em.	[Fe II] em.	Multi-core Na I	Near eclipsing source
CD-32 4371	M3I:	0.94				Gaia DR3 5594921650170191744
BD+53 2693	K2Ia	1.83				V2263 Cyg
HD 115336	K3.5Iab	2.18				Gaia DR3 5859054064419031040
HD 142696	M0Ib	1.25				Gaia DR3 5884691789303621504
V349 Car	M3Iab	1.22	X	weak	✓	EB signal offset from photocenter
V1092 Cen	M2.5Iab	10.26	X	X	X	Gaia DR3 5335719343117052544
TIC 44430172	M1Iab	2.65	X			EB signal offset from photocenter
Other hypothesized candidates						
Star	Spectral type	Period [d]	H em.	[Fe II] em.	Multi-core Na I	Notes
VV Cep	M2Ib+B2	~42	✓	✓	✓	V/R variations, VV Cep type

\* V340 Sge has a wide companion at 30 arcsec, but its light variations cannot be separated with TESS. The eclipses appear to be present in the full PSF of the RSG.

stars is uncertain. In Fig. B.10, we show a comparison of UV spectra of KQ Pup to  $\phi$  Per (Be+sdOB) and GG Car (B[e]sg). A detailed study of the population of hot components in VV Cephei systems is beyond the scope of this paper and will require new UV observations.

### 6.3. Implications for multiplicity of massive stars and evolution

From our results, it appears that at least 5 (FR Sct has a different classification) out of 44 Galactic binary RSGs (Healy et al. 2024) may have a third component, as revealed by TESS eclipses. This implies that many other RSG binaries must actually be hierarchical triple systems as well, just without eclipses. The ratio becomes even higher for VV Cephei RSGs - 2-4 out of 13 original VV Cephei stars (Cowley 1969) may be triples.

Ercolino et al. (2024) showed that binary interaction of (initially) wide RSG+B pairs can cause large blue loops in the HR diagram before exploding as various types of SN. Indeed, several post-RSG yellow hypergiants (YHG) showing signs of binary interaction were identified, most famously the recent transition of WOH G64 to YHG (Munoz-Sánchez et al. 2024), while suddenly showing VV Cephei properties. Likewise, some other YHGs are thought to be post-RSG objects and show signs of binary interaction, such as HD 144812, which has a disk hosting a companion (Kourniotis et al. 2025), which would also be similar to VV Cephei RSGs. Meanwhile, V772 Cen, one of the original VV Cephei RSGs, no longer shows the VV Cephei prop-

erties<sup>11</sup>. Thus, it appears that the VV Cephei phenomenon may be a sign of a transitory evolutionary phase, occurring only for part of the orbit for wider eccentric orbits (Balmer line emissions may disappear by apastron). For more evolved systems, as the orbit shrinks, the interaction becomes stronger and more frequent, eventually causing evolution toward different spectral types, in some cases very fast, as in the case of WOH G64. Furthermore, hierarchical triple RSG systems, such as possibly VV Cephei type, could very well be progenitors to high-mass Be/sdOB binaries (Reig 2011; Valli et al. 2025) upon RSG exploding as SN, while the ones without X-rays could evolve into Be+sdOB binaries.

## 7. Conclusions

In this work, we report the discovery of the first hierarchical triple RSG system, KQ Pup, consisting of an RSG (A) and two hot components (Ba+Bb) in a tight binary. This was accomplished by an innovative combination of several instruments and methods, some of them used in this way for an RSG system for the first time. We combined high-precision VLTI-GRAVITY astrometric measurements, enabled by detection of hydrogen Bry line in near-IR, with RV measurements, to determine orbital parameters and dynamical masses for the system. The derived masses agree with those estimated for KQ Pup A from asteroseismology and for KQ Pup Ba from evolutionary models.

<sup>11</sup> Archival spectra available at <https://archive.eso.org/scienceportal/home>

These results give an unexpected mass ratio for the system, with Ba+Bb components being more massive than the RSG component, i.e.,  $M_{\text{Ba+Bb}} \sim 14 M_{\odot}$  and  $M_A \sim 9 M_{\odot}$ , making the RSG a less-massive outer tertiary in the system, despite dominating the optical light. Such a configuration is compatible with MESA-MIST evolutionary models, yielding an approximate age of the system of  $\sim 30$  Myr.

Rather than direct mass transfer between the stellar components, the disk in the KQ Pup system (and likely also other VV Cephei binaries) is fueled by wind-RLOF from the dense RSG wind to the inner binary, as the strength and properties of Balmer lines strongly depend on the orbital phase, with the strongest Balmer emission near periastron. This is compatible with the detection of Bry feature, being the first such detection for a RSG system, which allowed us to uniquely determine dynamical masses. The interaction between the disk and the Bb companion may also play a role in the detection of Bry. The Bry line is routinely used for studying other types of interacting massive stars with VLTI-GRAVITY, including with relative astrometry (e.g., Frost et al. 2022; Klement et al. 2025).

The discovery of KQ Pup Bb was enabled primarily by the detection of eclipses in TESS light curves, and we also list other independent methods supporting its existence:

- TESS eclipses: we detected primary and secondary eclipses for KQ Pup in all 4 sectors (2019-2025). These eclipses have a period of  $P = 17.2596$  d and show an eccentric orbit. We tested representative Ba+Bb models in PHOEBE to estimate more properties of the inner binary and reproduce the observed light curve. The models favor a lower mass Bb (to agree with the RV scatter of Ba) and yield a lower limit on the eccentricity.
- V/R variations: with our newly taken high-cadence STELLA optical spectra, we observe variations of Balmer emission profiles on a similar timescale as the Ba+Bb orbit, i.e.,  $\sim 17$  d, especially for H $\beta$ .
- Bry: there are small departures of Bry positions from the A+B orbit, which could be compatible with the proposed orbit of Ba+Bb.
- mass ratio of A to Ba+Bb: the mere fact that the combined mass of Ba+Bb is higher than that of A can be explained only by a Bb component. If Ba on a wide orbit were a single component more massive than the A component, it would already have to be more evolved than the RSG component, unless significant mass transfer occurred.

Determining the nature of the population of binary hot components in RSG systems will require further study and modelling. For KQ Pup Ba, we find best-matching PoWR model with  $T_{\text{eff}} = 19\,900$  K,  $v \sin i \sim 190$  km s $^{-1}$  and  $\log(L) \sim 3.95$   $L_{\odot}$ , making it a fast-rotating ( $v_{\text{init}}/v_{\text{crit}} \sim 0.4$ ) B2 main-sequence star near TAMS. Most likely, KQ Pup Bb is also a main-sequence star with a minimum mass of  $\gtrsim 1.2 M_{\odot}$  rather than a stripped star, as no typical lines of stripped He-rich subdwarfs were detected. Overall, in the UV spectra, we find more similarities with B[e]sg binaries than Be+sdOB systems.

We also list several other candidates for eclipsing hierarchical triple RSG systems, which will require further observations. Our findings have important implications for the multiplicity of massive stars, as we have found evidence of a third component for about 10% known Galactic RSG binaries (e.g., Healy et al. 2024). Such a large number suggests that a large fraction of other RSG binaries also are, in fact, hierarchical triple systems. And in some of them, if similar to KQ Pup, more massive components could be hiding in light of the RSG component.

Our results demonstrate several methods to study such systems and detect new companions. New high-cadence spectroscopy would be sufficient to find more non-eclipsing candidates based on short-term V/R variations in VV Cephei systems. To determine more precise properties of hot components, including those of KQ Pup Ba+Bb, high-resolution, high-cadence observations in UV are required, such as with HST. For such systems, using VLTI-GRAVITY to study Bry line allows us to determine precise dynamical masses and study spatial properties of the companion at high-angular resolution. Meanwhile, future VLTI observations will allow us to constrain the dynamical masses of the system further, especially when combined with upcoming epoch astrometry from Gaia DR4.

*Acknowledgements.* We thank E. Paunzen for the first look at SMEI data for KQ Pup, and to Gregory Henry for providing the APT light curves. Discussions with A.K. Dupree and W.-R. Hamann are also acknowledged. DJ acknowledges support from the ESO Studentship. DJ and JK were partially supported by grant GA ČR 25-15910S. GGT is supported by the German Deutsche Forschungsgemeinschaft (DFG) under Project-ID 496854903 (SA4064/2-1, PI Sander), and acknowledges financial support by the Federal Ministry for Economic Affairs and Climate Action (BMWK) via the Deutsches Zentrum für Luft- und Raumfahrt (DLR) grant 50 OR 2503 (PI Sander). VR and AACS are supported by the German *Deutsche Forschungsgemeinschaft*, DFG in the form of an Emmy Noether Research Group – Project-ID 445674056 (SA4064/1-1, PI Sander). VR and AACS further acknowledges financial support by the Federal Ministry for Economic Affairs and Climate Action (BMWK) via the Deutsches Zentrum für Luft- und Raumfahrt (DLR) via the DLR grant 50 OR 2306 (PI Ramachandran/Sander). This project was co-funded by the European Union (Project 101183150 - OCEANS). Based on observations made with the Very Large Telescope Interferometer (VLTI) at the Paranal Observatory of European Southern Observatory (ESO). Based on data obtained with the STELLA robotic telescopes in Tenerife, an AIP facility jointly operated by AIP and IAC. Based on observations obtained at the Canada-France-Hawaii Telescope (CFHT) which is operated by the National Research Council of Canada, the Institut National des Sciences de l'Univers of the Centre National de la Recherche Scientifique of France, and the University of Hawaii. We acknowledge the use of TESS High Level Science Products (HLSP) produced by the Quick-Look Pipeline (QLP) at the TESS Science Office at MIT, which are publicly available from the Mikulski Archive for Space Telescopes (MAST). Funding for the TESS mission is provided by NASA's Science Mission directorate. Based on INES data from the IUE satellite. PLATOSpec was built and is operated by a consortium consisting of the Astronomical Institute ASCR in Ondrejov, Czech Republic (ASU), the Thüringer Landessternwarte (Thuringian State Observatory - Germany), the Universidad Católica in Chile (PUC - Chile), and minor partners include Masaryk University (Czechia), Universidad Adolfo Ibañez (Chile) and Institute for Plasma Physics of the Czech Academy of Sciences (Czechia). DP acknowledges financial support from the FWO in the form of a junior postdoctoral fellowship No. 1256225N. Financing for the modernisation and front end of the 1.52-m telescope was provided by ASU and personal costs were partly financed from grant LTT-20015. Financing for the construction of PLATOSpec was provided by the Free State of Thuringia, under the "Directive for the Promotion of Research PUC is acknowledging the support from ANID Fondecyt n. 1211162 and n. 1251299, and ANID QUIMAL ASTRO20-0025. Use of the 1.52-m telescope was made possible through an agreement between ESO and the PLATOSpec consortium. This research was supported by the 'SeismoLab' KKP-137523 Élvalon grant of the Hungarian Research, Development and Innovation Office (NKFIH) and by the LP2025-14/2025 Lendület grant of the Hungarian Academy of Sciences. This research made use of NASA's Astrophysics Data System Bibliographic Services, as well as of the SIMBAD and VizieR databases operated at CDS, Strasbourg, France.

## References

Ake, T. B. & Griffin, E., eds. 2015, *Astrophysics and Space Science Library*, Vol. 408, *Giants of Eclipse: The  $\zeta$  Aurigae Stars and Other Binary Systems*  
 Altamore, A., Giangrande, A., & Viotti, R. 1982, *A&AS*, 49, 511  
 Altamore, A., Rossi, C., Viotti, R., & Baratta, G. B. 1992, *A&AS*, 92, 685  
 Anugu, N., Baron, F., Gies, D. R., et al. 2023, *AJ*, 166, 78  
 Arcos, C., Kanaan, S., Chávez, J., et al. 2018, *MNRAS*, 474, 5287  
 Arroyo-Torres, B., Witkowski, M., Chiavassa, A., et al. 2015, *A&A*, 575, A50  
 Ash, A. L., Pinsonneault, M. H., Vrard, M., & Zinn, J. C. 2025, *ApJ*, 979, 135  
 Bailer-Jones, C. A. L., Rybizki, J., Fouesneau, M., Demleitner, M., & Andrae, R. 2021, *AJ*, 161, 147

Bányai, E., Kiss, L. L., Bedding, T. R., et al. 2013, MNRAS, 436, 1576

Bauer, W. H. & Bennett, P. D. 2000, PASP, 112, 31

Bernini-Peron, M., Marcolino, W. L. F., Sander, A. A. C., et al. 2023, A&A, 677, A50

Bernini-Peron, M., Sander, A. A. C., Ramachandran, V., et al. 2024, A&A, 692, A89

Bondi, H. & Hoyle, F. 1944, MNRAS, 104, 273

Bourges, L., Mella, G., Lafraisse, S., et al. 2017, VizieR Online Data Catalog: JMMC Stellar Diameters Catalogue - JSDC. Version 2 (Bourges+, 2017), VizieR On-line Data Catalog: II/346. Originally published in: 2014ASPC..485..223B

Brahm, R., Jordán, A., & Espinoza, N. 2017, PASP, 129, 034002

Caldwell, D. A., Tenenbaum, P., Twicken, J. D., et al. 2020, Research Notes of the American Astronomical Society, 4, 201

Choi, J., Dotter, A., Conroy, C., et al. 2016, ApJ, 823, 102

Conroy, K. E., Kochoska, A., Hey, D., et al. 2020, ApJS, 250, 34

Cowley, A. P. 1965, ApJ, 142, 299

Cowley, A. P. 1969, PASP, 81, 297

Cruzalèbes, P., Petrov, R. G., Robbe-Dubois, S., et al. 2019, MNRAS, 490, 3158

Daflon, S., Cunha, K., Smith, V. V., & Butler, K. 2003, A&A, 399, 525

Dai, M., Wang, S., & Jiang, B. 2025, MNRAS, 539, 1220

de Vries, N., Portegies Zwart, S., & Figueira, J. 2014, MNRAS, 438, 1909

Dommangé, J. & Nys, O. 2002, VizieR Online Data Catalog: CCDM (Components of Double and Multiple stars) (Dommangé+ 2002), VizieR On-line Data Catalog: I/269A. Originally published in: Observations et Travaux (in press)

Dorda, R. & Patrick, L. R. 2021, MNRAS, 502, 4890

Dorn-Wallenstein, T. Z., Levesque, E. M., Neugent, K. F., et al. 2020, ApJ, 902, 24

Dotter, A. 2016, ApJS, 222, 8

Dupree, A. K. 1986, ARA&A, 24, 377

Dupree, A. K. & Reimers, D. 1987, in Astrophysics and Space Science Library, Vol. 129, Exploring the Universe with the IUE Satellite, ed. Y. Kondo & W. Wamsteker, 321

Dupree, A. K., Strassmeier, K. G., Calderwood, T., et al. 2022, ApJ, 936, 18

Eggleton, P. P. 1983, ApJ, 268, 368

Ercolino, A., Jin, H., Langer, N., & Dessart, L. 2024, A&A, 685, A58

Fitzpatrick, E. L. 1999, PASP, 111, 63

Frost, A. J., Bodensteiner, J., Rivinius, T., et al. 2022, A&A, 659, L3

Gaia Collaboration, Brown, A. G. A., Vallenari, A., et al. 2021, A&A, 649, A1

Gaia Collaboration, Vallenari, A., Brown, A. G. A., et al. 2023, A&A, 674, A1

Goldberg, J. A., Joyce, M., & Molnár, L. 2024, ApJ, 977, 35

Goldberg, J. A., O'Grady, A. J. G., Joyce, M., et al. 2025, arXiv e-prints, arXiv:2505.18375

González-Riestra, R., Rossi, C., & Viotti, R. 2002, in Astronomical Society of the Pacific Conference Series, Vol. 261, The Physics of Cataclysmic Variables and Related Objects, ed. B. T. Gänsicke, K. Beuermann, & K. Reinsch, 281

González-Riestra, R., Rossi, C., & Viotti, R. F. 2003, A&A, 399, 681

González-Torà, G., Wittkowski, M., Davies, B., & Plez, B. 2024, A&A, 683, A19

Gosset, E., Hutsemekers, D., Surdej, J., & Swings, J. P. 1985, A&A, 153, 71

Gräfener, G., Koesterke, L., & Hamann, W. R. 2002, A&A, 387, 244

GRAVITY Collaboration, Abuter, R., Accardo, M., et al. 2017, A&A, 602, A94

Gustafsson, B., Edvardsson, B., Eriksson, K., et al. 2008, A&A, 486, 951

Hainich, R., Ramachandran, V., Shenar, T., et al. 2019, A&A, 621, A85

Harmanec, P., Yang, S., Koubský, P., et al. 2025, A&A, 699, A321

Healy, S., Horiuichi, S., Colomer Molla, M., et al. 2024, MNRAS, 529, 3630

Howell, S. B., Ciardi, D. R., Clark, C. A., et al. 2025, ApJ, 988, L47

Huber, D., Bedding, T. R., Stello, D., et al. 2011, ApJ, 743, 143

Humphreys, R. M. & Jones, T. J. 2022, AJ, 163, 103

Jordi, C., Gebran, M., Carrasco, J. M., et al. 2010, A&A, 523, A48

Joyce, M., Leung, S.-C., Molnár, L., et al. 2020, ApJ, 902, 63

Kashi, A. 2023, MNRAS, 523, 5876

Kiss, L. L., Szabó, G. M., & Bedding, T. R. 2006, MNRAS, 372, 1721

Kjeldsen, H. & Bedding, T. R. 1995, A&A, 293, 87

Klement, R., Rivinius, T., Baade, D., et al. 2025, A&A, 694, A208

Klement, R., Rivinius, T., Gies, D. R., et al. 2024, ApJ, 962, 70

Kloppenborg, B., Stencel, R., Monnier, J. D., et al. 2010, Nature, 464, 870

Kloppenborg, B. K., Stencel, R. E., Monnier, J. D., et al. 2015, ApJS, 220, 14

Kochanek, C. S., Shappee, B. J., Stanek, K. Z., et al. 2017, PASP, 129, 104502

Kourniotis, M., Kraus, M., Arias, M. L., & Cidale, L. S. 2025, MNRAS, 540, L28

Kozai, Y. 1962, AJ, 67, 591

Kraus, M., Oksala, M. E., Nickeler, D. H., et al. 2013, A&A, 549, A28

Labadie-Bartz, J., Carciofi, A. C., Henrique de Amorim, T., et al. 2022, AJ, 163, 226

Lajoie, C.-P. & Sills, A. 2011, ApJ, 726, 67

Lamers, H. J. G. L. M., Zickgraf, F.-J., de Winter, D., Houziaux, L., & Zorec, J. 1998, A&A, 340, 117

Lechien, T., de Mink, S. E., Valli, R., et al. 2025, arXiv e-prints, arXiv:2505.14780

Levesque, E. M. 2017, Astrophysics of Red Supergiants, 2514-3433 (IOP Publishing)

Lidov, M. L. 1962, Planet. Space Sci., 9, 719

Lightkurve Collaboration, Cardoso, J. V. d. M., Hedges, C., et al. 2018, Lightkurve: Kepler and TESS time series analysis in Python, Astrophysics Source Code Library, record ascl:1812.013

MacLeod, M., Blunt, S., De Rosa, R. J., et al. 2025, ApJ, 978, 50

Manset, N. & Donati, J.-F. 2003, in Society of Photo-Optical Instrumentation Engineers (SPIE) Conference Series, Vol. 4843, Polarimetry in Astronomy, ed. S. Fineschi, 425–436

Marchiano, P., Brandi, E., Muratore, M. F., et al. 2012, A&A, 540, A91

Meillard, A., Millour, F., Kanaan, S., et al. 2012, A&A, 538, A110

Mérand, A. 2022, in Society of Photo-Optical Instrumentation Engineers (SPIE) Conference Series, Vol. 12183, Optical and Infrared Interferometry and Imaging VIII, ed. A. Mérand, S. Sallum, & J. Sanchez-Bermudez, 121831N

Merc, J., Gális, R., & Wolf, M. 2019, Research Notes of the American Astronomical Society, 3, 28

Merloni, A., Lamer, G., Liu, T., et al. 2024, A&A, 682, A34

Mohamed, S. & Podsiadlowski, P. 2007, in Astronomical Society of the Pacific Conference Series, Vol. 372, 15th European Workshop on White Dwarfs, ed. R. Napiwotzki & M. R. Burleigh, 397

Montagès, M., Cannon, E., Lagadec, E., et al. 2021, Nature, 594, 365

Munari, U., Traven, G., Masetti, N., et al. 2021, MNRAS, 505, 6121

Munoz-Sánchez, G., Kalitsounaki, M., de Wit, S., et al. 2024, arXiv e-prints, arXiv:2411.19329

Muratorio, G., Viotti, R., Friedjung, M., Baratta, G. B., & Rossi, C. 1992, A&A, 258, 423

Naoz, S., Farr, W. M., Lithwick, Y., Rasio, F. A., & Teyssandier, J. 2013, MNRAS, 431, 2155

Neugent, K. F. 2021, ApJ, 908, 87

Neugent, K. F., Levesque, E. M., & Massey, P. 2018, AJ, 156, 225

Neugent, K. F., Levesque, E. M., Massey, P., & Morrell, N. I. 2019, ApJ, 875, 124

Neugent, K. F., Levesque, E. M., Massey, P., Morrell, N. I., & Drout, M. R. 2020, ApJ, 900, 118

O'Grady, A. J. G., O'Connor, B., Goldberg, J. A., et al. 2025, arXiv e-prints, arXiv:2505.18376

Ohnaka, K., Hofmann, K. H., Weigelt, G., et al. 2024, A&A, 691, L15

Okazaki, A. T. 2007, in Astronomical Society of the Pacific Conference Series, Vol. 367, Massive Stars in Interactive Binaries, ed. N. St. -Louis & A. F. J. Moffat, 485

Oskinova, L. M. 2016, Advances in Space Research, 58, 739

Pantaleoni González, M., Maíz Apellániz, J., Barbá, R. H., & Negueruela, I. 2020, Research Notes of the American Astronomical Society, 4, 12

Patrick, L. R., Lennon, D. J., Schootemeijer, A., et al. 2025, A&A, 700, A36

Patrick, L. R. & Negueruela, I. 2024, Bulletin de la Société Royale des Sciences de Liège, 93, 173

Patrick, L. R., Thilker, D., Lennon, D. J., et al. 2022, MNRAS, 513, 5847

Paxton, B., Bildsten, L., Dotter, A., et al. 2011, ApJS, 192, 3

Paxton, B., Cantiello, M., Arras, P., et al. 2013, ApJS, 208, 4

Paxton, B., Marchant, P., Schwab, J., et al. 2015, ApJS, 220, 15

Pigulski, A. & Michalska, G. 2007, Information Bulletin on Variable Stars, 5757, 1

Pollmann, E. & Bennett, P. 2020, jaavso, 48, 118

Porter, A., Blundell, K., & Lee, S. 2022, MNRAS, 509, 1720

Porter, A., Grant, D., Blundell, K., & Lee, S. 2021, MNRAS, 501, 5554

Prša, A., Conroy, K. E., Horvat, M., et al. 2016, ApJS, 227, 29

Prša, A., Kochoska, A., Conroy, K. E., et al. 2022, ApJS, 258, 16

Puebla, R. E., Hillier, D. J., Zsargó, J., Cohen, D. H., & Leutenegger, M. A. 2016, MNRAS, 456, 2907

Ramachandran, V., Hamann, W. R., Oskinova, L. M., et al. 2019, A&A, 625, A104

Reig, P. 2011, Ap&SS, 332, 1

Reimers, D. 1975, Mémoires of the Societe Royale des Sciences de Liège, 8, 369

Ricker, G. R., Winn, J. N., Vanderspek, R., et al. 2015, Journal of Astronomical Telescopes, Instruments, and Systems, 1, 014003

Rivinius, T. & Klement, R. 2024, arXiv e-prints, arXiv:2411.06882

Rossi, C., Altamore, A., Baratta, G. B., Friedjung, M., & Viotti, R. 1992, A&A, 256, 133

Rossi, C., Villada, M., Viotti, R., & Baratta, G. B. 1998, in ESA Special Publication, Vol. 413, Ultraviolet Astrophysics Beyond the IUE Final Archive, ed. W. Wamsteker, R. Gonzalez Riestra, & B. Harris, 353

Rubio, A. C., Carciofi, A. C., Bjorkman, J. E., et al. 2025, arXiv e-prints, arXiv:2502.11626

Saladino, M. I. & Pols, O. R. 2019, A&A, 629, A103

Sana, H., de Mink, S. E., de Koter, A., et al. 2012, Science, 337, 444

Sander, A., Shenar, T., Hainich, R., et al. 2015, A&A, 577, A13

Sharma, A. N., Bedding, T. R., Saio, H., & White, T. R. 2022, MNRAS, 515, 828

Smartt, S. J., Eldridge, J. J., Crockett, R. M., & Maund, J. R. 2009, MNRAS, 395, 1409

Strassmeier, K. G., Granzer, T., Weber, M., et al. 2004, Astronomische Nachrichten, 325, 527

Strassmeier, K. G., Granzer, T., Weber, M., et al. 2010, Advances in Astronomy, 2010, 970306

Toonen, S., Portegies Zwart, S., Hamers, A. S., & Bandopadhyay, D. 2020, A&A, 640, A16

Valli, R., de Mink, S. E., Justham, S., et al. 2025, arXiv e-prints, arXiv:2505.08857

van Leeuwen, F. 2007, A&A, 474, 653

van Leeuwen, F., Evans, D. W., Grenon, M., et al. 1997, A&A, 323, L61

van Loon, J. T., Cioni, M. R. L., Zijlstra, A. A., & Loup, C. 2005, A&A, 438, 273

Vink, J. S., de Koter, A., & Lamers, H. J. G. L. M. 2001, A&A, 369, 574

Wang, L., Gies, D. R., Peters, G. J., et al. 2021, AJ, 161, 248

Weber, M., Granzer, T., & Strassmeier, K. G. 2012, in Society of Photo-Optical Instrumentation Engineers (SPIE) Conference Series, Vol. 8451, Software and Cyberinfrastructure for Astronomy II, ed. N. M. Radziwill & G. Chiozzi, 84510K

Weber, M., Granzer, T., Strassmeier, K. G., & Woche, M. 2008, in Society of Photo-Optical Instrumentation Engineers (SPIE) Conference Series, Vol. 7019, Advanced Software and Control for Astronomy II, ed. A. Bridger & N. M. Radziwill, 70190L

Winecki, D. & Kochanek, C. S. 2024, ApJ, 971, 61

Wolf, M., Harmanec, P., Božić, H., et al. 2021, A&A, 647, A97

Xiong, Q., Li, T., Yu, J., et al. 2025, ApJ, 984, 65

Yu, J., Bedding, T. R., Stello, D., et al. 2020, MNRAS, 493, 1388

<sup>1</sup> Department of Theoretical Physics and Astrophysics, Faculty of Science, Masaryk University, Kotlářská 2, 611 37, Brno, Czech Republic

e-mail: jadloovsky@mail.muni.cz

<sup>2</sup> European Southern Observatory (ESO), Karl-Schwarzschild Str. 2, D-85748, Garching bei München, Germany

<sup>3</sup> Konkoly Observatory, HUN-REN Research Centre for Astronomy and Earth Sciences, MTA Centre of Excellence, Konkoly-Thege Miklós út 15-17, H-1121, Budapest, Hungary

<sup>4</sup> MTA–HUN-REN CSFK Lendület "Momentum" Stellar Pulsation Research Group, Konkoly-Thege Miklós út 15-17, H-1121, Budapest, Hungary

<sup>5</sup> Eötvös Loránd University, Institute of Physics and Astronomy, H-1117 Pázmány Péter sétány 1/A, Budapest, Hungary

<sup>6</sup> Argelander Institut für Astronomie, Auf dem Hügel 71, DE-53121 Bonn, Germany

<sup>7</sup> Zentrum für Astronomie der Universität Heidelberg, Astronomisches Rechen-Institut, Mönchhofstr. 12-14, 69120 Heidelberg, Germany

<sup>8</sup> Universität Heidelberg, Interdisziplinäres Zentrum für Wissenschaftliches Rechnen, 69120 Heidelberg, Germany

<sup>9</sup> Yunnan Observatories, Chinese Academy of Sciences (CAS), Kunming 650216, Yunnan, China

<sup>10</sup> Leibniz-Institut für Astrophysik Potsdam (AIP), An der Sternwarte 16, D-14482 Potsdam, Germany

<sup>11</sup> Max Planck Institute for Extraterrestrial Physics (MPE), Giessenbachstrasse 1, D-85748, Garching bei München, Germany

<sup>12</sup> Institute for Physics and Astronomy, University Potsdam, 14476 Potsdam, Germany

<sup>13</sup> Institute of Astronomy, KU Leuven, Celestijnenlaan 200D, 3001 Leuven, Belgium

<sup>14</sup> Max-Planck-Institut für Astrophysik, Karl-Schwarzschild-Str. 1, 85748 Garching b. München, Germany

<sup>15</sup> Facultad de Ingeniería y Ciencias, Universidad Adolfo Ibáñez, Av. Diagonal las Torres 2640, Peñalolén, Santiago, Chile

<sup>16</sup> Millennium Institute for Astrophysics, Santiago, Chile

<sup>17</sup> Thüringer Landessternwarte Tautenburg, Sternwarte 5, 07778 Tautenburg, Germany

<sup>18</sup> Department of Electrical Engineering and Center of Astro Engineering of Pontificia Universidad Católica de Chile, Av. Vicuña Mackenna 4860, Santiago, Chile

<sup>19</sup> Astronomical Institute, Czech Academy of Sciences, Fričova 298, 251 65 Ondřejov, Czech Republic

## Appendix A: Observing logs for KQ Pup

In Table A.1, we list our VLTI-GRAVITY observations. In Table A.2, we list properties of VLTI calibrators, including parameters of MARCS spectra used to calibrate the flux of calibrator (Gustafsson et al. 2008). The obtained spectral transfer function was used to calibrate the flux of our science target. Lastly, in Table A.3, we list results obtained from fitting the Bry in our VLTI dataset when fitted per epoch.

Additionally, we also analyzed the atmospheric extension of KQ Pup A, following a similar workflow as in Jadlovský et al (in preparation). We fitted a uniform disk (UD) model to CO molecular bands  $^{12}\text{C}^{16}\text{O}$  (2-0) at  $2.29\ \mu\text{m}$  and  $^{12}\text{C}^{16}\text{O}$  (3-1) at  $2.32\ \mu\text{m}$  and compared to the photospheric diameter. In all 3 VLTI epochs, the obtained radii are similar and show an average CO atmospheric extension of  $\sim 1.13\ R_\star$ .

**Table A.1.** Lists of observations KQ Pup taken with VLTI-GRAVITY. All were taken at the smallest VLTI configuration, A0 B2 D0 C1, at high resolution and split polarization.

Date	Time [UT]	Exposure [s]	Seeing ["]	$\tau_0$ [ms]
2024-12-04	04:35:02	3.0	0.4	4.63
2025-01-28	02:52:58	3.0	0.96	4.9
2025-03-06	03:00:11	3.0	1.22	5.2

**Table A.2.** Properties of the calibrators based on Bourges et al. (2017), while the right part of the table shows properties of MARCS models Gustafsson et al. (2008) used for flux calibration (solar metallicity).

Calibrator	Sp. Type	LDD [mas]	UDK [mas]	$T_{\text{eff}}$ [K]	$\log g$
HD 58215	K4III	$2.54 \pm 0.25$	2.48	4000	1.5
d Vel	G6III	$1.70 \pm 0.15$	1.66	4500	2.0

**Table A.3.** Results obtained from fitting of Bry line in PMOIRE, listing the angular diameter  $\theta_{\text{A,UD}}$  of KQ Pup A (KQ Pup B considered unresolved), flux contribution  $f_B$  of KQ Pup B, full width at half maximum (FWHM) of Bry line, and positions of Bry recovered from relative astrometry.

Date	$\theta_{\text{A,UD}}$ [mas]	$f_B$	$f_{\text{Bry}}$	FWHM <sub>Bry</sub> [nm]	$x_B$ [mas]	$y_B$ [mas]
2024-12-04	5.85	$\sim 0$	0.033	1.27	$-3.25_{\pm 0.51}$	$-4.58_{\pm 0.14}$
2025-01-28	5.83	$\sim 0$	0.034	1.01	$-4.13_{\pm 0.12}$	$-3.41_{\pm 0.14}$
2025-03-06	5.94	$\sim 0$	0.027	1.35	$-5.15_{\pm 0.22}$	$-2.35_{\pm 0.19}$

## Appendix B: Auxiliary plots for KQ Pup and other candidates

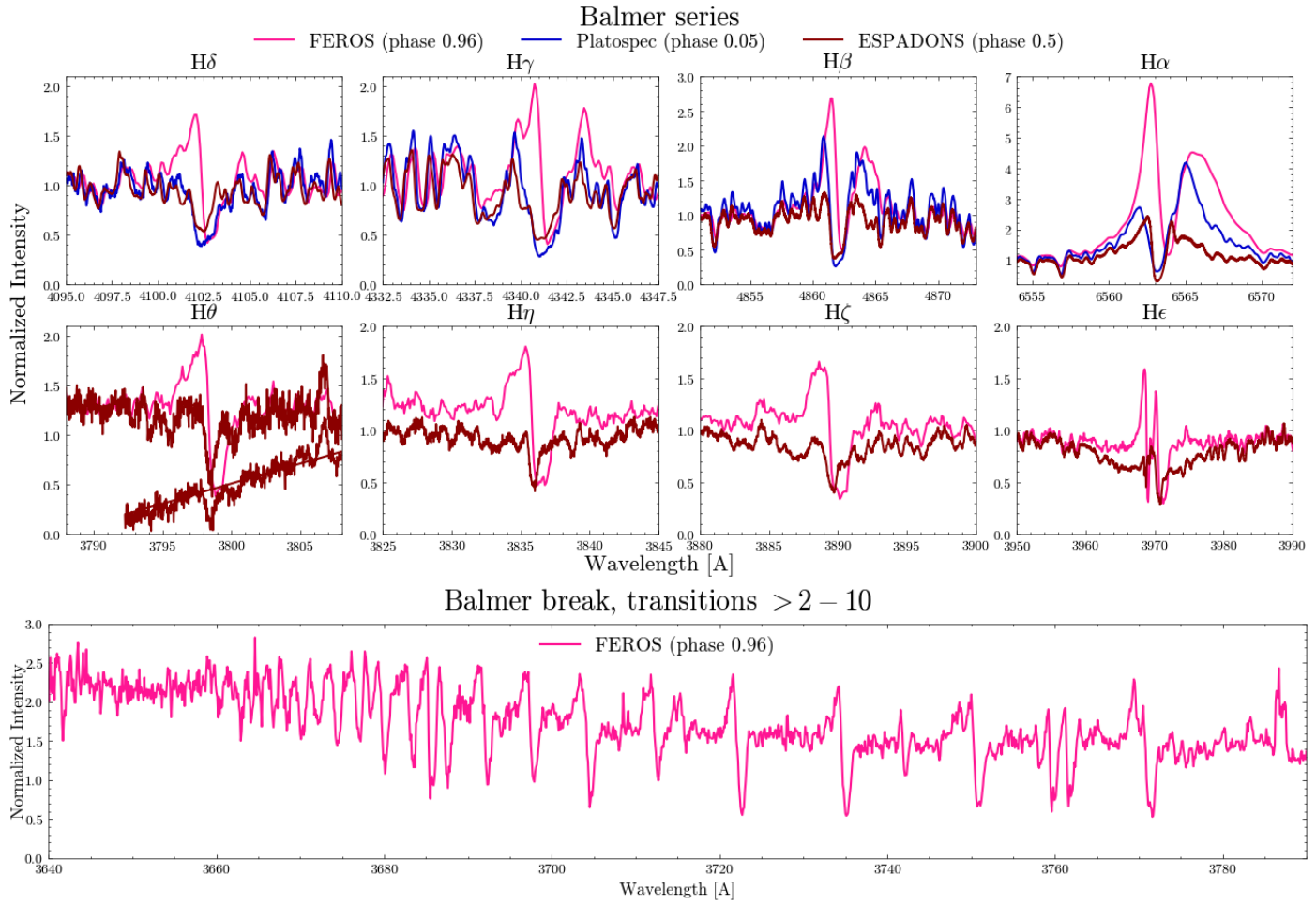


**Fig. B.1.** Balmer series, from H $\alpha$  (2-3) to H $\theta$  (2-10), based on ESPADONS and PLATOSpec for different AB orbital phases. While the majority of the optical spectrum is dominated by the RSG, the Balmer lines form near the hot component. Single RSGs usually do not show the highest Balmer transitions. The lower plot shows all Balmer lines up to the Balmer break near periastron. Archival optical spectra also show that the V/R ratio is dependent on orbital phase of 26 yr (e.g., Rossi et al. 1998). We note that the central sharp feature in H $\epsilon$  is due ISM, and the wide depression is likely instrumental effect in ESPADONS spectra.

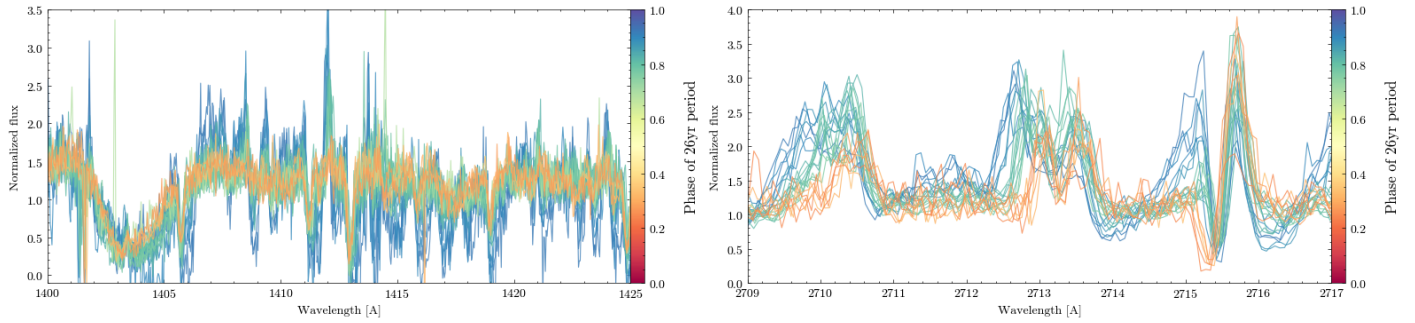


**Fig. B.2.** Important features from the IUE spectra. *Left panel:* Resonance and narrow lines in the SWP region, colored based on the 26-year period. We observe the narrow lines broadening and deepening near periastron. *Right panel:* Emission and P Cygni profiles in LWP. We see that for most of the 26-year orbit, the spectra show regular P Cygni profiles, and their cores move toward the longer wavelengths, while the emission lines move in the opposite direction. Near periastron, some of the P Cygni profiles appear reversed.

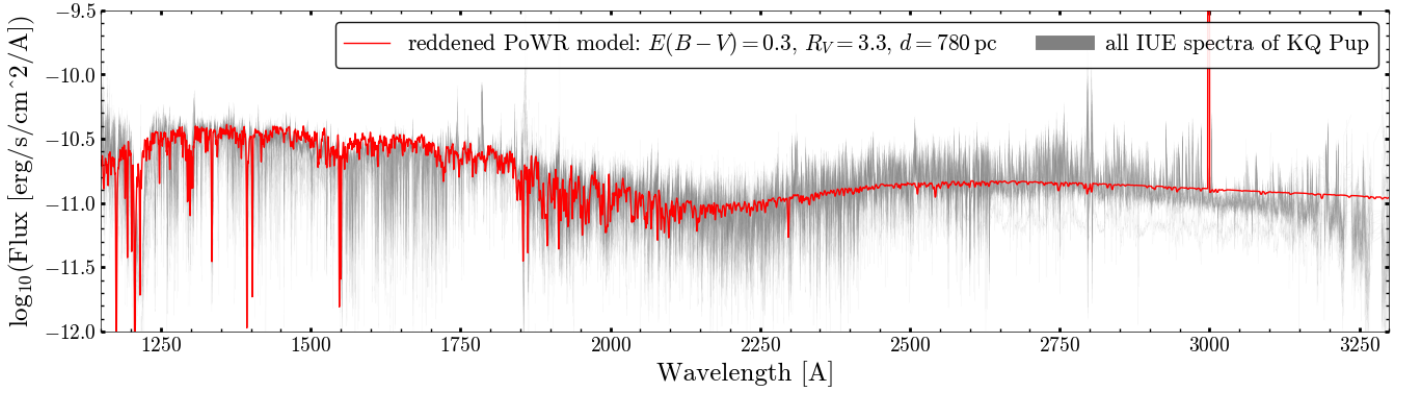


**Fig. B.3.** Reddened PoWR model compared to all IUE SWP and LWP/R binned spectra. The model agrees with the observations for reddening of  $E(B-V) = 0.30$  with  $R_V = 3.3$  and assuming the distance of 780 pc (BJ21).

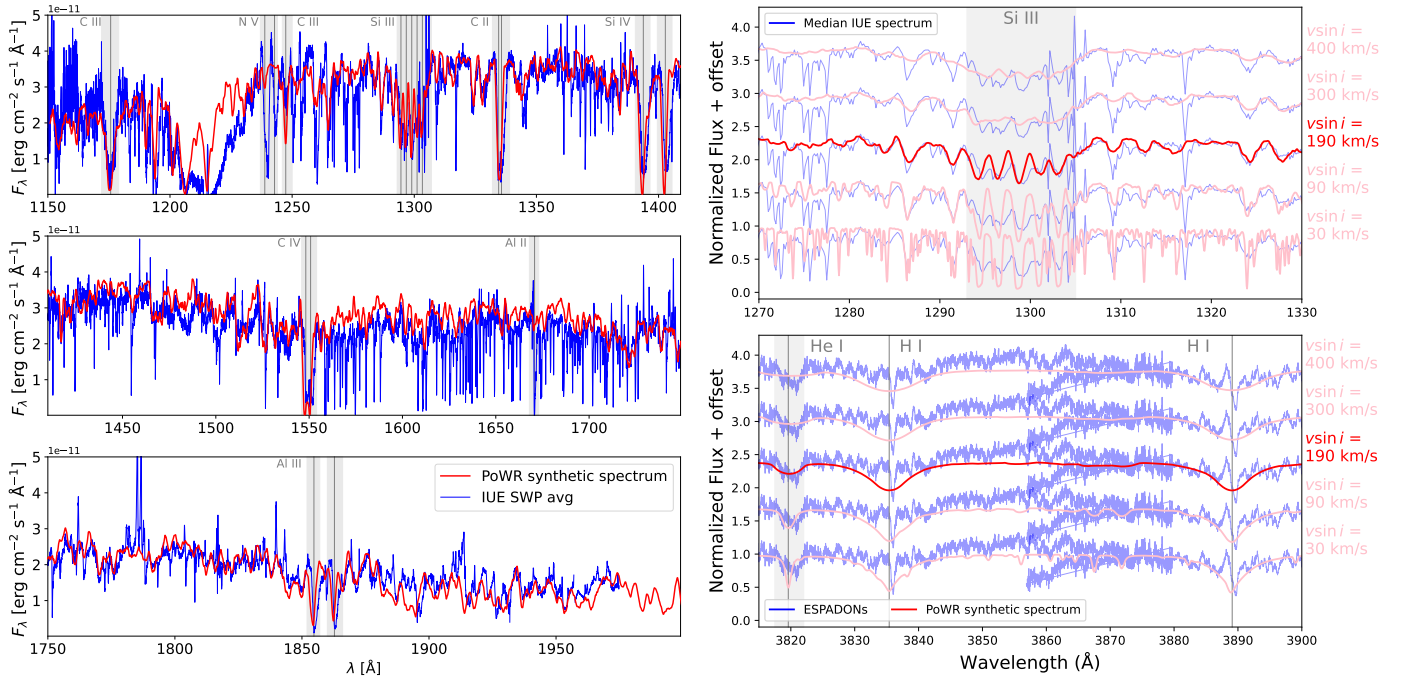


**Fig. B.4.** *Left panel:* Best-fit of the PoWR model atmosphere to KQ Pup IUE data, showing regions of the SWP spectra. *Right panel:* Example of determining  $v \sin i$  from the IUE SWP spectra. Rotationally-broadened He I line at 3819 Å is also reproduced by the fit; other He I below 4000 Å do not appear to show such broadening, likely due to their proximity to H $\gamma$  and H $\zeta$ .

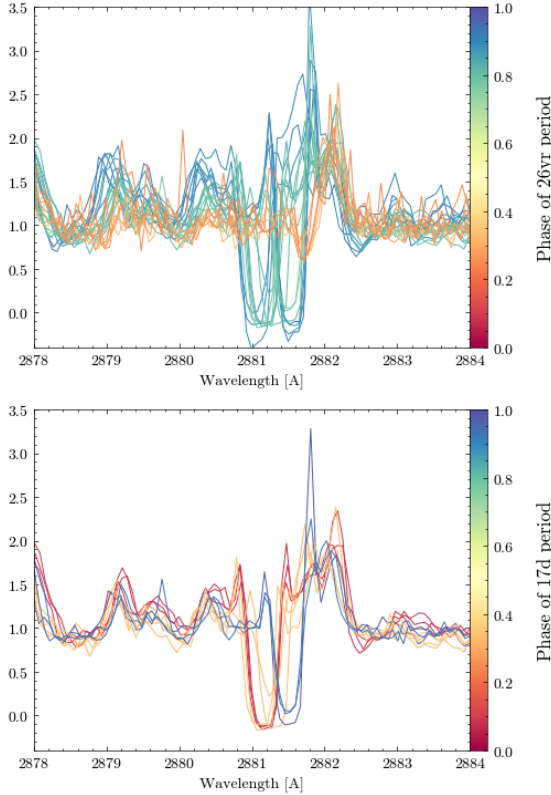


**Fig. B.5.** Example of variable shell profiles - the line shows a deep absorption profile near periastron. For the rest of the phase, it is a redshifted emission. In the upper panel, we see it colored based on the 26 yr orbital period. In the lower panel, it is colored based on the 17d period (for observations between phases 0.7-0.85), suggesting a relation to the 17d period.

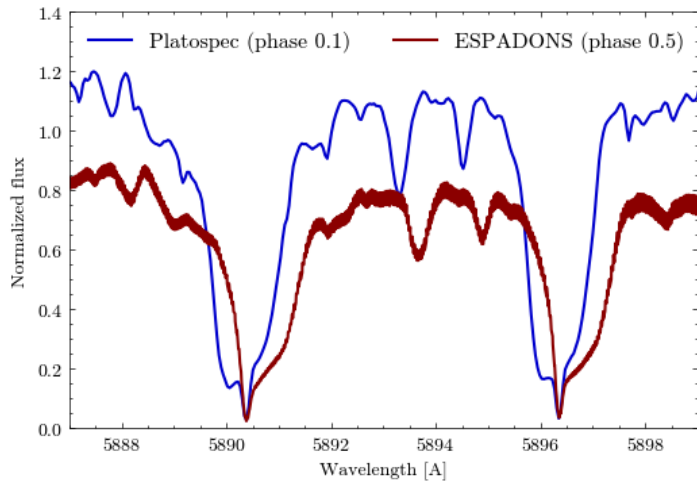


**Fig. B.6.** Na I doublet for KQ Pup near periastron and apastron. We see a clear relation to the 26-year A+B orbital period, with the sharp absorption component staying in place.

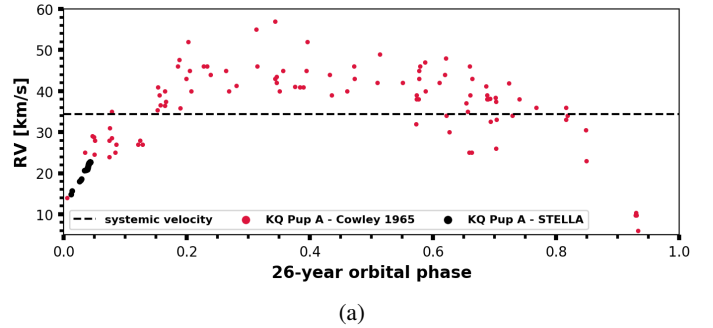


**Fig. B.7.** Phased RV of KQ Pup A compared to the archival RV data from 1918-1964 (Cowley 1965). The new STELLA data confirms the validity of the revised 26-year orbital period determined by González-Riestra et al. (2002).

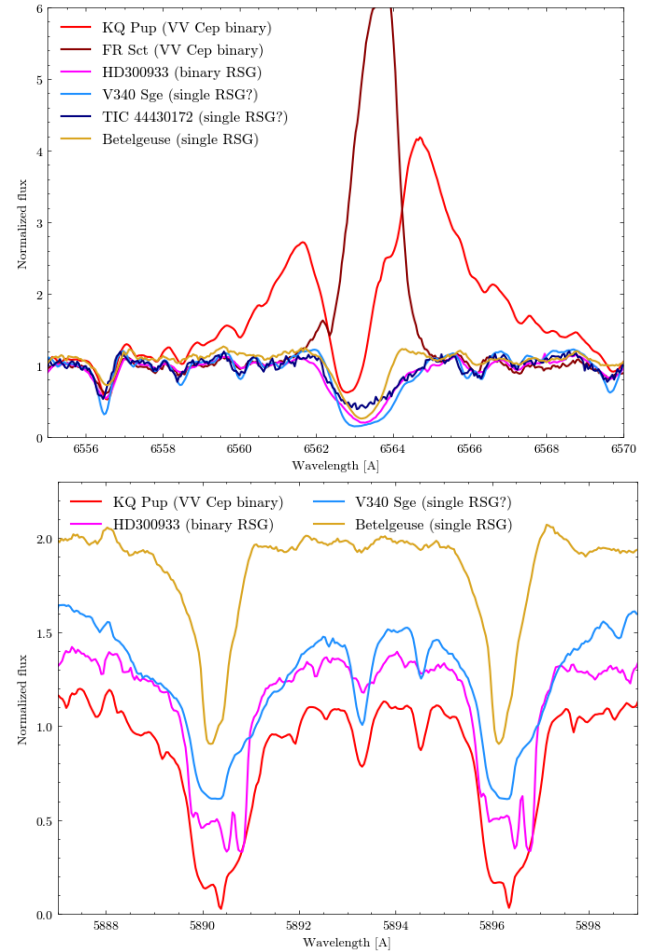


**Fig. B.8.** *Upper panel:* Comparison of H $\alpha$  line for our promising candidates, using PLATOSpec spectra. We can see that only the VV Cephei type RSGs show the Balmer emission. Single RSGs have a deep absorption. *Lower panel:* The same, but for Na I doublet, which shows multiple cores for binary RSGs. We compare to Betelgeuse, a well-known RSG without a hot massive B-type companion. We also show V340 Sge, one of our candidates, which doesn't have a known companion, but the Na I line shows very broad components.

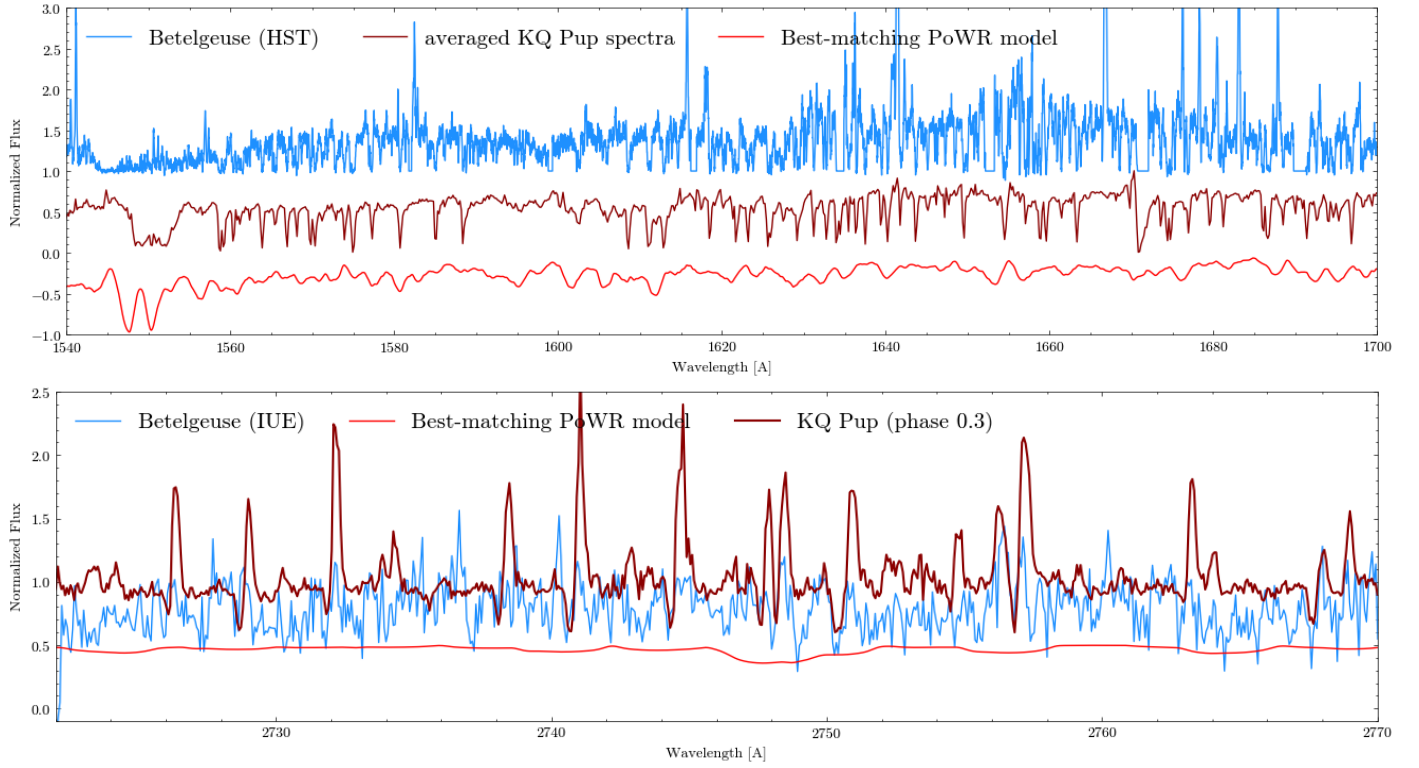


**Fig. B.9.** *Upper panel:* Comparison of KQ Pup IUE SW spectra to Betelgeuse (HST), also showing comparison to our best-fit PoWR model, each vertically shifted. The narrow lines are not reproduced by our high-rotating PoWR model for KQ Pup, while many of the narrow lines (e.g., Fe III) in the KQ Pup spectrum appear to also be present in the spectrum of Betelgeuse; thus, the majority of these lines likely do not correspond to KQ Pup Bb and form in the wind of the RSG. The HST spectrum was downloaded from the ASTRAL database [https://archive.stsci.edu/prepds/astral/summaries/h\\_alp\\_ori\\_summary.html](https://archive.stsci.edu/prepds/astral/summaries/h_alp_ori_summary.html). *Lower panel:* The same, but for Fe II P Cygni profiles in the LWP/R region and compared to the IUE spectrum of Betelgeuse. Absorption part of P Cygni profiles is also present in the spectrum of Betelgeuse; therefore, these lines clearly form in the ionized wind of the RSG.

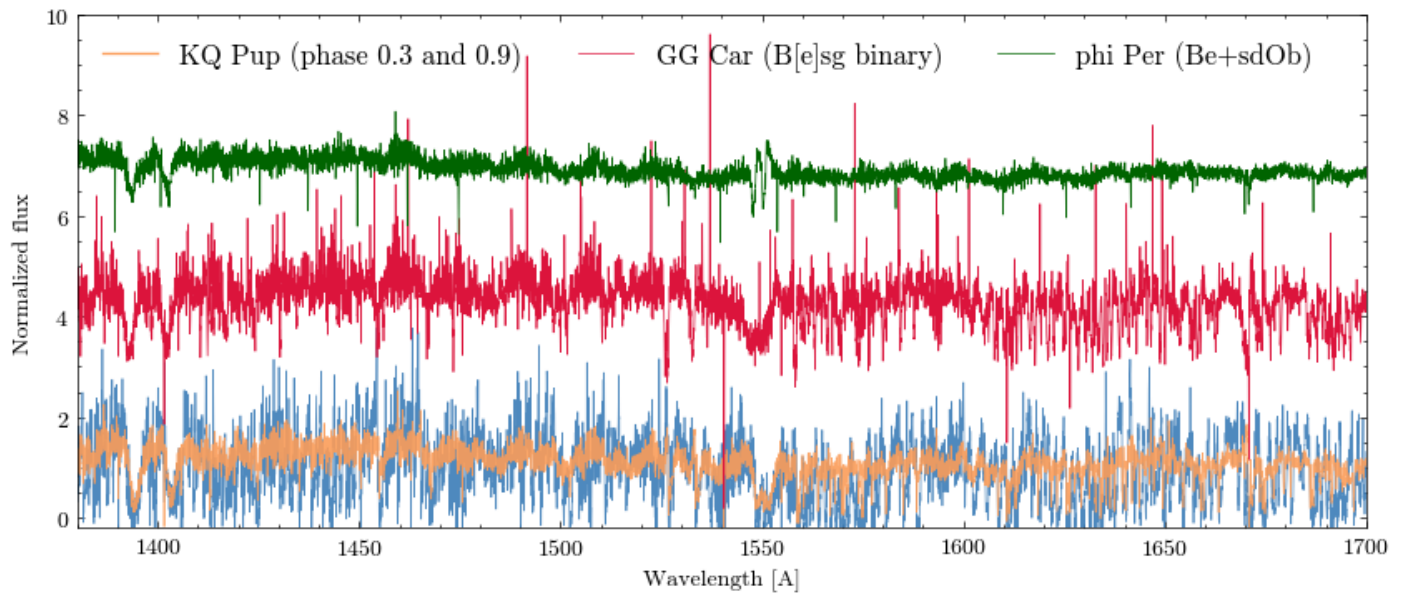


**Fig. B.10.** Comparison of KQ Pup (for epochs 0.3, orange, and 0.9, blue) to a typical Be+sdOB ( $\phi$  Per) and a known B[e]sg binary GG Car, using the IUE SWP spectra.

## Appendix C: Raw TESS data for KQ Pup and other promising candidates

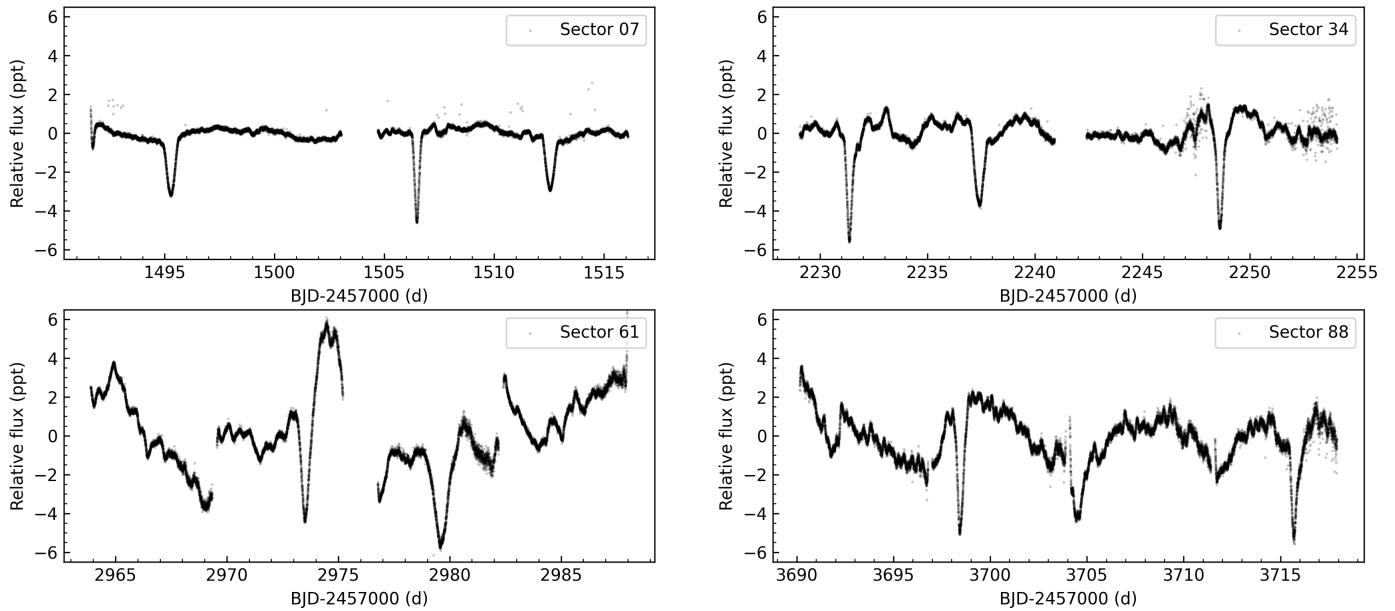


**Fig. C.1.** SPOC data (120 s exposures) for the 4 available sectors in the TESS dataset - sectors 7 (January 2019), 34 (January 2021), 61 (January 2023), and 88 (January 2025).

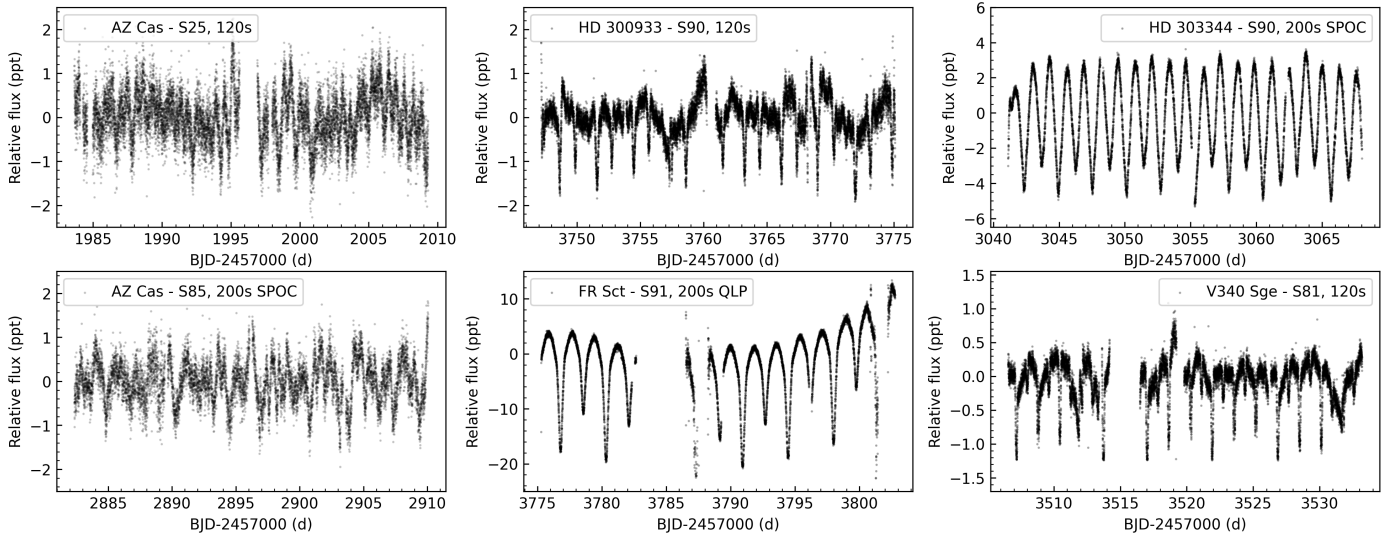


**Fig. C.2.** Examples of TESS data (for selected sectors) for the other promising candidates. We used 200 s or 120 s (where available) cadences. We show two sectors for AZ Cas, whose classification as an EB is uncertain.

## Appendix D: Stellar evolutionary models

### Appendix D.1: Preliminary constraints on the timescales and masses

Using stellar evolution models from MIST (Dotter 2016), assuming solar metallicity and initial rotation of 40% critical, we can infer the age of the system as well as constrain the mass of KQ Pup Ba. To do this, we use the data available (VLTI global+RV fit) in Table 1, which gives us  $M_A \sim 7.6 - 10.9 M_\odot$ . Accounting for wind-mass loss until halfway through core-He burning, the stellar evolution models suggest initial masses  $M_{A,i} \sim 7.6 - 11.6 M_\odot$ . For example, for  $M_A = 9.1 M_\odot$ , we obtain  $M_{A,i} \simeq 9.3 M_\odot$ . For such a star to be observed as a red supergiant, it must have an age  $\sim 18.7 - 46.9$  Myr (Fig. D.1).

Within this age constraint, we can infer the possible ranges of initial masses that KQ Pup Ba and KQ Pup Bb must have, assuming both Ba and Bb are main-sequence stars, with Ba being the more massive one. The observed values are likely to be smaller by  $\lesssim 0.5 M_\odot$  due to wind-mass loss between ZAMS and the moment at which the system is observed. We also assume that the triple system has evolved coevally, and that KQ Pup Ba and Bb have not experienced any form of mass-transfer.

Under these assumptions, we can constrain the minimum mass of Bb for it to have successfully reached the main-sequence by the time of the observation. For our range of ages, Bb must have initial masses above  $\sim 1.2 - 1.5 M_\odot$  (MIST, Dotter 2016). As Bb cannot hold more than half the mass of the Ba+Bb system, we derive that  $M_{Bb} \leq \frac{1}{2}M_{Ba+Bb} \sim \frac{1}{2}qM_{A,i}$ . For the given range of uncertainties in  $M_A$ , this yields  $1.2M_\odot \lesssim M_{Bb} \lesssim 8.1 M_\odot$  (see Fig. D.1).

For the mass of Ba, we note that being a more massive star in the binary, we can constrain its minimum mass to  $M_{Ba} \geq \frac{1}{2}M_{Ba+Bb} \sim \frac{1}{2}qM_A$ . For its maximum mass, we note that it cannot be more massive than KQ Pup A at ZAMS, otherwise it would have evolved to a RSG, and therefore  $M_{Ba} \lesssim M_{A,i}$ . Within the current uncertainties on  $M_A$ , the mass constraint of Ba is  $5.7 M_\odot \lesssim M_{Ba} \lesssim 11.6 M_\odot$  (see Fig. D.1). These values are compatible with those derived from asteroseismic measurements (see Sect. 3.1).

The orbital period of 17.26 d is such that RLOF only occurs after one of the two stars leaves the main-sequence (see Fig. D.1). It is worth noting that this does not necessarily prove that we are observing the system before such an event. Indeed, if mass-transfer has already occurred, KQ Pup Ba may actually be the initially less massive companion that accreted a lot of mass, while KQ Pup Bb is the initially more massive companion, which is now partially stripped. The observations do not provide evidence supporting this scenario (see Sect. 4), and future observations of Ba alone cannot constrain this scenario well. For example, if future observations classify Ba as a Be star, which is evidence that the star has accreted material and is spinning rapidly, this may have been driven by the accretion of material from the winds of KQ Pup A, instead of mass transfer from the initially more massive but now dim Bb. The non-zero eccentricity of Ba+Bb is also noteworthy, as mass-transfer typically circularizes orbits, but it may also have been driven by eccentricity pumping from the interaction with the RSG winds.

### Appendix D.2: Extended atmosphere

We can estimate the local density that the extended structure of KQ Pup A would have close to the Ba+Bb binary. We follow Ercolino et al. (2024) and construct an extended envelope assum-

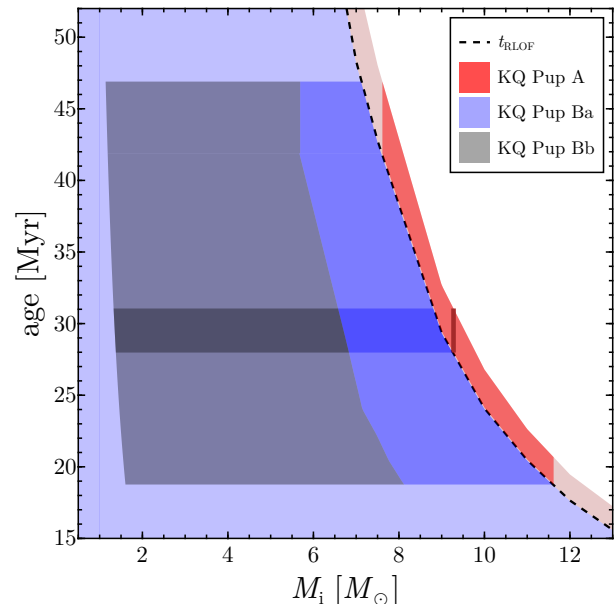


**Fig. D.1.** Age-mass diagram from the MIST stellar models (Dotter 2016). Different regions mark how a single star of given initial mass and age would appear, either as a main-sequence star (light blue) or a RSG (light red). The region highlighted in red shows the parameter space in age and mass for KQ Pup A. Similarly, the region highlighted in blue and gray shows the parameter space for KQ Pup Ba and Bb, within the constraints of the mass and age of KQ Pup A and the assumption that Ba is more massive than Bb. The regions with darker highlighting show the mass constraints for KQ Pup Ba and Bb assuming the mean value for the mass of KQ Pup A. The dashed line reports the age range for which higher masses would have left the main-sequence and trigger Case B RLOF, assuming an orbital period of 17.26 d.

ing a quasi-hydrostatic, isothermal stratification with turbulent pressure using a single-star of  $M \sim 11.6 M_\odot$  halfway through core-helium burning, with  $\log L/L_\odot = 4.5$ ,  $T_{\text{eff}} = 3420$  K and  $R = 526 R_\odot$  (cf. the asteroseismology estimates in Table 1). While the photospheric radius is about  $\sim 5$  times smaller than the orbital separation at periastron ( $\sim 2700 R_\odot$ ), the extended hydrostatic layers may be much larger (Ercolino et al. 2024).

Assuming that the inner binary is outside the low-density hydrostatic layers of KQ Pup A, we stitch a  $\beta$ -law wind structure (with  $\beta = 5$  and  $v_\infty = 25 \text{ km s}^{-1}$ ) above the sonic point ( $v_{\text{sound}} = 5 - 15 \text{ km s}^{-1}$ ) of the extended atmosphere (see Ercolino et al. 2024). With this, we note that the density contrast of the material swept by the inner-binary at periastron passage with KQ Pup A is about one order of magnitude higher than at apastron. The Bondi-Hoyle accretion (Bondi & Hoyle 1944) from KQ Pup A to the inner-binary is roughly around 10% of the mass-loss rate from KQ Pup A during periastron passage, while it can be significantly higher at apastron (due to the smaller velocities). However, we note that the low velocity and relatively high mass of the binary result in an accretion radius that is similar to the orbital separation, meaning that the Bondi-Hoyle model is not suitable to address the accretion of material by the Ba+Bb binary. Indeed, if the strength of the Balmer emission traces the accreted material from KQ Pup A, the Bondi-Hoyle mechanism would imply the opposite behavior. This therefore strengthens the scenario that KQ Pup A is undergoing wind-RLOF with the inner Ba+Bb binary (Mohamed & Podsiadlowski 2007).